REVIEW

Check for updates

Recent advances in upgrading CO_2 to C_{3+} products *via* electrochemical and complementary engineering†

Xian Zhong, [ab] Hong-Jie Peng, [a] Chuan Xia (ID) *[bd] and Xinyan Liu (ID) *[ac]

Upgrading CO_2 to various carbon-containing products through renewable electrochemical routes offers a promising solution to achieve a "Net Zero" and circular economy. Multicarbon C_{3+} products are especially energy-rich and economically valuable. However, due to the diverse possibilities of C−C coupling and the complexities of reaction pathways, the efficient and selective electrochemical reduction of CO_2 to C_{3+} products remains a tremendous challenge. Summarizing the latest advances in generating C_{3+} products from CO_2, this review focuses on both key material development and process design in electrochemical and complementary engineering approaches. For the methodologies involving only electrochemical reactions, we categorize them based on the catalysts adopted, summarizing the specific design strategies and mechanistic understandings of copper and non-copper catalysts, respectively. To further improve the efficiency of C_{3+} synthesis, the concept of "electrochemical + X" is introduced. "X" herein refers to a complementary sector to direct CO_2 electrolysis, encompassing the homogeneous non-electrocatalytic reactions in a one-pot electrochemical process and the sequential thermochemical or biological processes after electrochemical CO_2 conversion. Lastly, we discuss the challenges of pure electrochemical as well as "electrochemical + X" approaches and outline promising future directions. We believe that this review contains a comprehensive summary of the means to

[a] *Institute of Fundamental and Frontier Sciences, University of Electronic Science and Technology of China, Chengdu 611731, P. R. China. E-mail: xinyanl@uestc.edu.cn*

[b] *School of Materials and Energy, University of Electronic Science and Technology of China, Chengdu 611731, P. R. China. E-mail: chuan.xia@uestc.edu.cn*

[c] *Key Laboratory of Quantum Physics and Photonic Quantum Information, Ministry of Education, University of Electronic Science and Technology of China, Chengdu 611731, P. R. China*

[d] *Yangtze Delta Region Institute (Huzhou), University of Electronic Science and Technology of China, Huzhou 313001, P. R. China*

† Electronic supplementary information (ESI) available. See DOI: https://doi.org/10.1039/d4ta03088e

Xian Zhong

Xian Zhong graduated from Chang'an University with a bachelor's degree in 2021. Now she is pursuing a master's degree under the joint supervision of Dr Xinyan Liu and Prof. Chuan Xia at the University of Electronic Science and Technology of China (UESTC). Her research interests mainly focus on first-principles calculations for applications such as electrocatalytic CO_2 reduction, water splitting, and high-energy secondary batteries.

Hong-Jie Peng

Dr Hong-Jie Peng is a Professor at the Institute of Fundamental and Frontier Sciences (IFFS), University of Electronic Science and Technology of China (UESTC). He obtained B.S. and PhD degrees at the Department of Chemical Engineering, Tsinghua University, in 2013 and 2018, respectively. He was a postdoctoral fellow at SUN-CAT Center, Stanford University, during 2018–2020. He was selected as a Highly Cited Researcher from 2019 to 2023 by Clarivate Analytics. His current research interests are advanced energy chemistry and energy materials, including high-energy rechargeable batteries, renewable electrocatalysis, theoretical tools, and data-driven methods.

This journal is © The Royal Society of Chemistry 2024

J. Mater. Chem. A, 2024, **12**, 19663–19684 | **19663**

optimize for C_{3+} compounds, and can motivate researchers to develop innovative strategies to further enhance C_{3+} production efficiency, paving the way towards the ultimate renewable-driven chemical industries.

1. Introduction

The increase in carbon dioxide (CO_2) emissions inevitably induces global warming and detrimental threats to the environment.[1,2] Based on this aspect, upgrading CO_2 to value-added chemical feedstocks through renewable approaches remains extremely valuable, as it presents a sustainable approach to alleviate environmental stress and complete the anthropogenic carbon cycle.[3] Various technologies of CO_2 reutilization have been developed in recent years, including chemical,[4] thermochemical,[5,6] biochemical,[7,8] photochemical,[9–11] and electrochemical methods.[12–15] Among these technologies, the electrochemical CO_2 reduction reaction (eCO_2RR) powered by electricity from sustainable sources emerges as a promising candidate, due to its mild reaction conditions (*e.g.* room temperature and ambient pressure) and the substantially lower cost of renewable electricity. As the eCO_2RR consumes renewable energies while producing multiple base chemicals,[16] it is anticipated to supplement or even replace the current fossil-resource-based chemical manufacture, manifesting great potential to achieve "Net Zero" industrial CO_2 emissions.

Remarkable progress has been reported for the eCO_2RR to C_1 and C_2 hydrocarbons and oxygenates (*e.g.*, carbon monoxide (CO),[17–19] methanol (CH_3OH),[20–22] ethanol (CH_3CH_2OH)[23–25] and ethylene (C_2H_4)[26–28]), where outstanding reaction activities and selectivities can be achieved. Compared to their C_1 or C_2 counterparts, C_{3+} products usually exhibit higher energy densities and are more economically valuable. For instance, 1-propanol ($CH_3CH_2CH_2OH$) possesses high volumetric energy density (27.0 kJ mL^{-1}) and research octane number (118). The most typical C_4 monohydric alcohol, 1-butanol

($CH_3CH_2CH_2CH_2OH$), exhibits even higher volumetric energy density (29.2 kJ mL^{-1}).[29] Both C_{3+} alcohols are promising substitutes for petroleum-derived gasoline. Along with other C_3 and C_4 products such as allyl alcohol, acetone, and propionaldehyde,[30] they serve as important raw chemicals for fine chemical industries. Long-chain aliphatic and aromatic hydrocarbons, though challenging to produce from CO_2, are desirable synthetic fuels due to their high heat value and lower volatility compared to light hydrocarbons/oxygenates, and remain more compatible with the existing fuel storage and transportation infrastructures.[29,31,32] If the scope of C_{3+} products is further expanded to nutrients such as saccharides, amino acids, and lipids, electrochemical CO_2 upgrading will further provide a sustainable avenue towards synthetic foods to cope with the growth of the global population.[33,34] However, electrochemically converting CO_2 to C_{3+} products with practically relevant efficiency still remains a formidable challenge owing to the complexity in reaction pathways and the insufficiency in key materials and new process design.

In this work, we focus on recent advances in upgrading CO_2 to C_{3+} products through direct electrochemical and "electrochemical + X" approaches, where "X" refers to complementary engineering with homogeneous reactions, thermochemical conversions, and biological processes (Fig. 1). We begin with a brief introduction on the principles of the eCO_2RR, followed by C_{3+} formation mechanisms with a primary focus on the most widely adopted copper (Cu)-based catalysts. Then, we summarize the design and optimization principles of both Cu-based and non-Cu catalysts to enhance their catalytic activities towards C_{3+} chemicals in direct electrochemical CO_2 conversion. The latest research progress in coupling the eCO_2RR with

Chuan Xia

Dr Chuan Xia is a Professor of Materials and Energy at the University of Electronic Science and Technology of China (UESTC). His group focuses on developing novel catalysts and device architectures that can be applied in electrocatalysis. He has won the J. Evans Attwell-Welch postdoctoral fellowship (2019), Best Applied Paper Award of AIChE (2020), and Falling Walls Science Breakthroughs of the Year Award (2022), Top 10 News Stories of Scientific and Technological Progress in China (2022), Sichuan Youth May Fourth Medal (2023), and Chinese Chemical Society Young Chemist Award (2023). More information about his research can be found here: https://www.chuan-lab.com.

Xinyan Liu

Dr Xinyan Liu is a Research Professor at the Institute of Fundamental and Frontier Sciences (IFFS), University of Electronic Science and Technology of China (UESTC). Having obtained her bachelor's and PhD degree from Tsinghua University and Stanford University in 2013 and 2018 respectively, she has also worked at Meta Inc. for two years as a Research Data Scientist before she joined full time at UESTC. Dr Liu's research interest has been mainly focused on energy chemistry-related interdisciplinary study combining theoretical simulations and artificial intelligence, such as electrocatalysis, catalyst high-throughput screening, and battery prognosis.

19664 | *J. Mater. Chem. A*, 2024, **12**, 19663–19684

This journal is © The Royal Society of Chemistry 2024
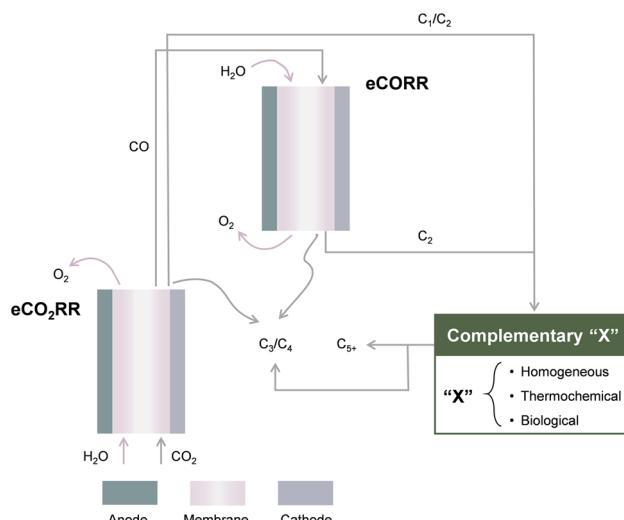
Fig. 1 Schematic illustration of direct electrochemical approaches (eCO$_2$RR and eCORR) and "electrochemical + X" approaches for upgrading CO$_2$ to C$_{3+}$ products.

other complementary engineering approaches, as well as the significance of such a combinatorial "electrochemical + X" strategy in achieving high C$_{3+}$ production efficiency, is then presented. Lastly, we conclude this work by providing a perspective on challenges and opportunities for both approaches, hoping to shed light on future research studies.

2. Direct electrochemical approaches

2.1. Principles of the eCO$_2$RR

For CO$_2$ upgrading to C$_3$ and C$_4$, it is viable to adopt direct electrochemical approaches through the eCO$_2$RR in an electrolysis system (Fig. 1). The eCO$_2$RR at the cathode is paired with oxidative reactions, normally the oxygen evolution reaction, at the anode. The electrolysis system can be designed in a one-pot or sequential fashion. The latter one in most cases consists of two electrolyzers in series;[35] where CO$_2$ reduces to CO in the first and the subsequent electrochemical CO reduction reaction (eCORR) take place in the second. The advantages of sequential design primarily lie in possibilities to optimize catalytic materials and reaction environments separately to maximize the efficiency of CO$_2$-to-CO conversion and the eCORR. For instance, the bulk and local electrolyte pH have been experimentally observed and theoretically validated to largely influence the product selectivities of the eCO$_2$RR/eCORR. Alkaline conditions have been demonstrated to promote the eCORR towards C$_{2+}$ multicarbon products with exceptional selectivity.[36–42] Nevertheless, direct eCO$_2$RR in alkaline solutions suffers from severe reactions between CO$_2$ and hydroxide, as well as the resultant decrease in local pH and decrease in carbon efficiency. The sequential electrolysis system design allows for addressing such a dilemma.

For the catalysts at the cathode side, metallic Cu and Cu-based materials have been intensively investigated for the eCO$_2$RR/eCORR in a direct electrocatalytic process and remain as the most well-known catalysts to drive the formation of C$_{2+}$ products.[16,43] Despite the great progress in improving the activity and selectivity of the eCO$_2$RR/eCORR towards C$_2$ products, strategies for enhancing carbon-chain growth to C$_{3+}$ products remain limited. In an early study, Hori *et al.* reported *n*-PrOH as an eCO$_2$RR product on Cu with a faradaic efficiency (FE) of 4.2% at a potential of −1.4 V *vs.* the normal hydrogen electrode (NHE) in KClO$_4$,[44] which establishes a C$_3$ production baseline on Cu. As CO* (* refers to a surface adsorption site) has been probed as a key surface intermediate for C–C coupling,[45–47] challenges of efficient C$_{3+}$ production include both insufficient surface coverage of CO*[48,49] and the large number of competing reaction pathways against C$_{3+}$ formation.[50] For instance, the inadequate stabilization of C$_2^*$ intermediates on pristine Cu surfaces leads to species desorption rather than further inter-molecular coupling with CO*. In addition, the coupling of certain intermediates always suffers from competitions with corresponding hydrogenation/protonation reactions under reductive conditions. Therefore, it remains essential to acquire a deeper understanding of the reaction mechanisms and develop catalysts capable of stabilizing key C$_2^*$ intermediates and favoring the specific coupling pathway towards C$_{3+}$.

2.2. C$_3$ formation mechanisms through the eCO$_2$RR

As Cu and oxide-derived Cu (OD-Cu) catalysts have been investigated the most for the eCO$_2$RR to C$_{2+}$ products, the majority of mechanistic studies leveraging theoretical computations or spectroscopic characterization also focus on these catalysts. Compared to C$_1$ and C$_2$ products, the C$_3$ formation mechanism remains more elusive due to the complexity in reaction pathways and the large number of possible steps (>10^3) involved in the entire reaction network. Enlightened by the widely recognized CO* dimerization mechanism to yield OCCO* as a common precursor for C$_2$ formation in the eCO$_2$RR, some density functional theory (DFT)-based attempts have been used to investigate the sequential (first, 2CO* → OCCO* + *, and then, OCCO* + CO* → OCCOCO* + *) or concerted (3CO* → OCCOCO* + 2*) CO* trimerization mechanism,[51–53] where the OCCOCO* trimer was proposed as the initial C$_3$ backbone for further reduction. However, recent studies by Abild-Pedersen *et al.*[54] and López *et al.*[55] both argued that the high activation barrier (ΔG_a of at least 1 eV at −0.9 V *vs.* the reversible hydrogen electrode (RHE, pH 7), relative to 3CO*) for this process on Cu(100) or OD-Cu makes it less favorable than other C$_2$–C$_1$ coupling steps, and that the direct trimerization is kinetically inaccessible as the protonation of the negatively charged OCCO* dimer dominates over the OCCO* + CO* coupling under reducing conditions. To validate the direct trimerization mechanism, spectroscopic evidence for the OCCOCO* trimer or its mono-hydrogenated derivatives can be valuable and is still currently lacking.

Alternatively, statistical analyses of experiments and DFT computations were combined to balance the efficiency and accuracy of mechanism exploration, unveiling new mechanistic insights. Abild-Pedersen *et al.*[54] first correlated the C$_2$ and C$_3$ formation rates based on the pioneering work of the eCO$_2$RR on

Cu single-crystal substrates by Hori et al.,[56] revealing the higher possibilities of late C_2 intermediates (e.g. hydrocarbons C_2H_x, where x = 1–3, or mono-oxygenates such as acetaldehyde CH_3CHO) to participate in C_3 formation than late C_1 intermediates (e.g. CH_x). In addition, the correlations of 1-propanol with C_2H_4 or ethanol formation exhibit great differences regarding the correlation coefficient as well as the Cu facets, implying the existence of at least two possible parallel reaction pathways towards C_3 (Fig. 2a). Through the analysis of explicitly calculated barriers for all coupling steps between CO* and the likely C_2H_x intermediates, they identified the coupling of HCCH* and CO* (HCCH* + CO* → CHCHCO* + *) as the most kinetically feasible step to compete with the corresponding hydrogenation on both flat Cu(100) and stepped Cu(511) facets featuring four-fold square sites. Specifically, facets combining (100)-like square sites and step sites, such as Cu(511), were found to exhibit notably lower HCCH*–CO* coupling barriers (ΔG_a = 0.51 eV at −0.9 V vs. RHE (pH 7)) than flat Cu(100) (ΔG_a = 0.80 eV at −0.9 V vs. RHE). This finding well explains the experimentally observed higher C_3 selectivity on stepped Cu(100) facets.[56] In addition, they further elucidated the feasibility of CO*–CH_3CHO* coupling (CH_3CHO* + CO* → $OCCHOCH_3^*$ + *) under alkaline conditions. Thanks to the substantial stabilization of an interfacial electric field on its transition state, this step exhibits a low barrier of ΔG_a = 0.61 eV at −0.6 V vs. RHE (pH 13) on Cu(100), which opens up a supplementary pathway towards C_3 on non-stepped Cu surfaces. As the (100)-like square sites are identified to be crucial for C–C coupling, Tsai et al. investigated the strain effect on Cu(100) model surfaces and found that biaxial strains, namely compression along one axis and elongation along the other, significantly lowered C_2–CO coupling barriers although two different C_2 intermediates of CCH* and CCOH* were considered.[57] The symmetry distortion from standard square sites to a rectangle or parallelogram site was shown to enable two scales for stabilizing the C_2^* and CO* adsorbates, respectively.

Since OD-Cu has been experimentally probed as an excellent catalyst promoting C_3 formation, theoretical efforts have been devoted to this specific system as well.[55,58] By devising a divide-and-conquer strategy that combines reaction network graphs, DFT calculations equipped with an implicit solvation model and a voltage polarization correction, and model co-reduction experiments, López et al. thoroughly examined the reaction thermodynamics and kinetics of 586 C_1–C_2 coupling steps and identified the coupling between C_2 hydrocarbons (e.g. CH_2CH^*) and C_1 mono-oxygenates (e.g. CO* and CHO*) as the most likely step (Fig. 2b).[55] Although the proposed intermediates to derive C_3 backbones are slightly different from those identified by Abild-Pedersen et al.,[54] this distinction could be attributed to the OD-Cu model considered for DFT calculations, where the Cu sites are polarized and thus different from the metallic sites in pure Cu models. Nevertheless, both studies identified a late C_2^* hydrocarbon intermediate as the key precursor for C_3 products in the eCO$_2$RR. While the previous work focused only on the C_3 backbone,[54] López et al. further explained the absence of propylene ($CH_3CH{=}CH_2$) in eCO$_2$RR products on routine Cu-based catalysts, which was ascribed to the inaccessible allyl alkoxy ($CH_2CHCH_2O^*$) intermediate as a kinetic trap.

In addition to DFT calculations, in situ spectroscopic observations provide experimental evidence to elucidate the C_3 formation mechanism. Employing isotopic labeling and in situ surface enhanced infrared absorption spectroscopy, Xu et al. investigated alkaline eCORR behaviors on OD-Cu with an addition of CH_3CHO in the electrolyte, revealing that CO attacks the carbonyl carbon of CH_3CHO during the coupling and the carbon from CO ends up in the hydroxymethyl (–CH_2OH) group of the 1-propanol product.[59] Interestingly, only a small fraction of C_3 was observed to come from CH_3CHO + CO coupling, while the majority remained as the result of self-coupling of CO. This suggested that there is an intermediate that forms before CH_3CHO, and can be derived from both CH_3CHO and CO. This intermediate was then proposed to be methylcarbonyl (CH_3CO^*), and the possibility of it acting as a precursor for C_3 formation is also supported by López et al.'s calculation results, as the coupling barrier between CH_3CO^* and CHO* could be as low as 0.32 eV.[55] So far, the in situ spectroscopic evidence is mostly obtained for the coupling step involving a C_2 oxygenate intermediate. The in situ characterization of the C_2 hydrocarbon-dominated cross-coupling mechanism, however, still remains limited.

The aforementioned mechanistic studies shed light on the C_3 formation mechanism during the eCO$_2$RR or eCORR on Cu-based catalysts, greatly promoting the rational design of catalytic materials and reactors to optimize C_3 yields. Yet it is still arguable which pathway is the most dominant and what the most crucial C_2 intermediate is. As C_2 formation could proceed via multiple pathways, the dominance of which is dependent on the potential, microenvironment, and catalytic surface, the governing C_3 formation pathways are anticipated to be dynamic as well. More in-depth theoretical and in situ/operando spectroscopic investigations would be necessary. Moreover, while Cu is focused on in the current mechanistic investigations, other catalysts may exhibit distinctive reaction mechanisms. In the next sections, we will discuss the strategies to further improve Cu-based catalysts and the efforts in seeking for alternative non-Cu catalysts.

2.3. Cu-based catalysts

As Cu-based materials are recognized as the most widely adopted catalysts for direct eCO$_2$RR or eCORR to C_{3+} chemicals, a variety of strategies have been proposed to regulate the nature and number of Cu active sites. Furthermore, catalyst engineering is often combined with reaction microenvironment modulation, synergistically shifting the concentration and/or coverage of key reaction intermediates (e.g. CO) to the optimal range for selective C_{3+} formation. Overall, these strategies can be categorized as micro-/nanostructure engineering, defect engineering, oxidation state regulation, and foreign element regulation. In addition, the rare case of selective eCO$_2$RR to C_3 by single-site Cu catalysts is also discussed.

2.3.1. Micro-/nanostructure engineering. Regarding the structural engineering of pristine Cu catalysts, we first revisit the series of single-crystal-Cu studies by Hori et al.[56,60] Substantial improvements in C_3 selectivity could be achieved by

19666 | J. Mater. Chem. A, 2024, 12, 19663–19684

This journal is © The Royal Society of Chemistry 2024
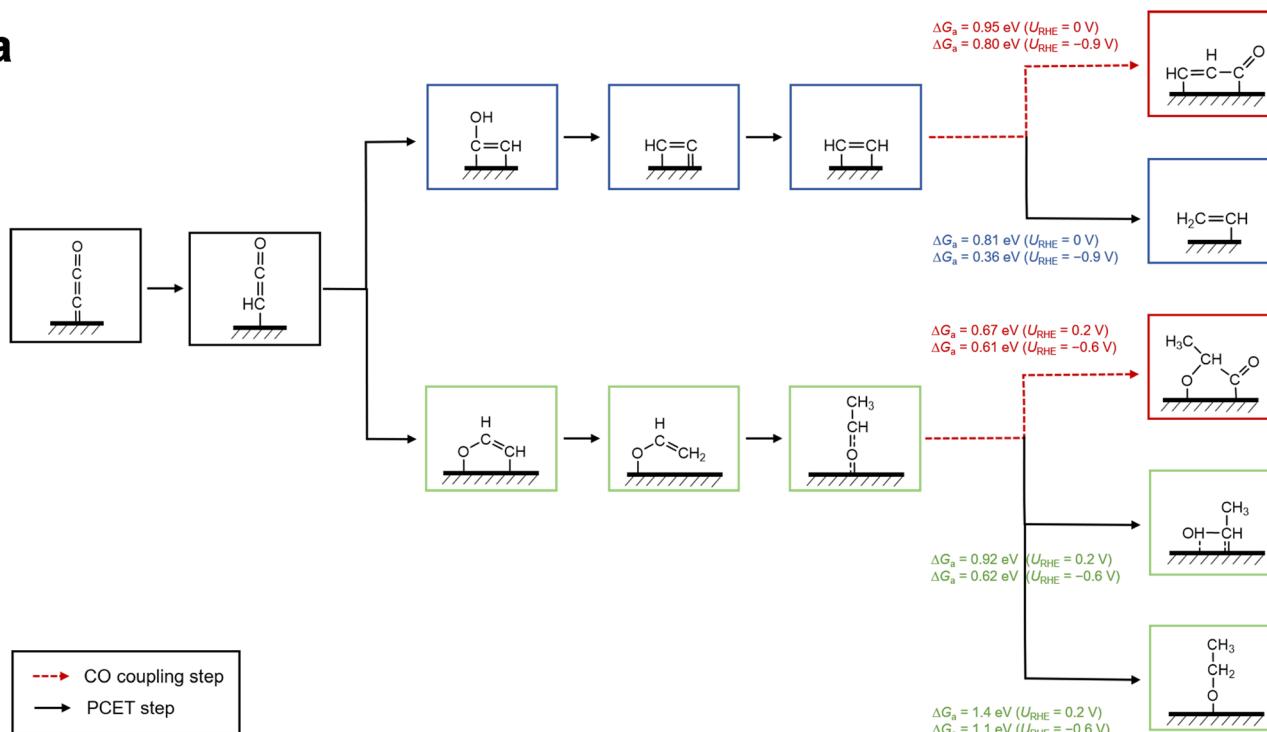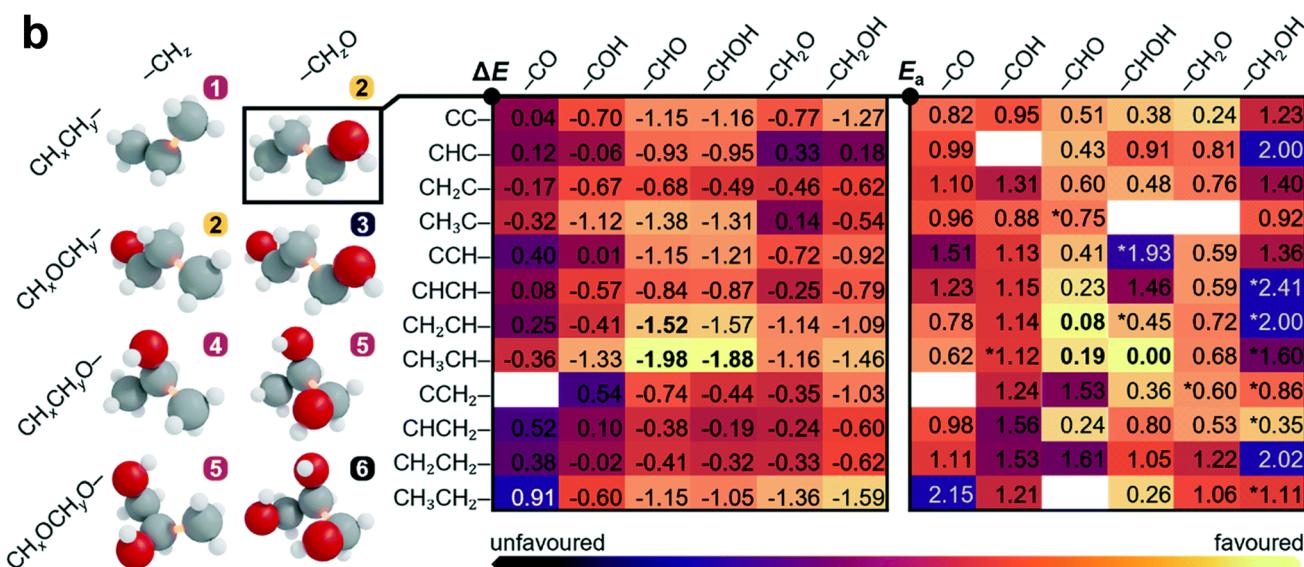
Fig. 2 C_3 formation mechanisms through the eCO$_2$RR on Cu and OD-Cu. (a) CO coupling mechanisms with late C_2 species such as HCCH* and CH$_3$CHO* to yield C_3 species (red), as well as the corresponding competing protonation steps of HCCH* (blue) and CH$_3$CHO* (green) that result in C_2 species such as ethylene and ethanol. DFT-calculated barrier ΔG_a is presented at two typical potentials vs. RHE (U_{RHE}). The presented data were reproduced from ref. 54 for the Cu(100) surface. (b) Typical $C_xH_yO_z$ backbones, and reaction and activation electronic energies (ΔE and E_a) for CH$_x$CH$_y$−CH$_2$O coupling steps on an OD-Cu surface model. The most likely steps are indicated in bold. Adapted from ref. 55 with permission from The Royal Society of Chemistry.

replacing polycrystalline Cu with single-crystal Cu(S)-[$n(100) \times (111)$] electrodes (including 1-propanol, propionaldehyde (CH$_3$CH$_2$CHO), and allyl alcohol (CH$_2$=CHCH$_2$OH)) at a constant current density of 5 mA cm^{-2} in an electrolyte of 0.1 M KHCO$_3$.[56] The single-crystal Cu electrode follows the microfacet notation proposed by Somorjai et al.,[61] and Cu(S)-

[$n(100) \times (111)$] refers to the Cu(100) facet modified by close-packed (111) steps. The fact that the best C_3 FE of 12% can be achieved on Cu(711) with a moderate density of step sites points out the significance of both (100)-like terrace and (111) step sites. While the former type of site is essential for selective eCO$_2$RR to C_2 hydrocarbon intermediates, the coupling of these

This journal is © The Royal Society of Chemistry 2024

J. Mater. Chem. A, 2024, 12, 19663–19684 | 19667

C_2 hydrocarbon fragments with CO was theoretically predicted to be more facile on under-coordinated sites.[54] The adoption of single-crystal substrates is, however, not practical for industrial-scale catalytic processes, due to the limited scalability of single-crystal material fabrication. Although the possibility of scalable synthesis of single-crystal metal foil has been recently showcased,[62,63] a great number of pieces of single-crystal Cu foil exhibited strong tendency to reconstruct under routine eCO_2RR conditions.[64] Therefore, alternative approaches to tailor active site types and distributions on Cu catalysts are required.

Since the general understanding on nanocatalysts has revealed that a decrease in nanoparticle size gives rise to an increase in step site densities,[65] it becomes straightforward to adopt Cu nanoparticles (NPs) and other nanostructures to enrich under-coordinated sites in the eCO_2RR. Moreover, coating nano-particulate Cu catalysts onto the gas diffusion layer (GDL) or integrating them into a membrane electrode assembly (MEA) is also rather convenient, endowing these approaches with desirable applicability in practical electrolyzers. For instance, Cuellar et al. investigated the particle size effect of four commercial Cu powders loaded on the GDL and demonstrated the advantage of CO as a reactant over CO_2 in improving the selectivity towards both C_2 and C_3.[35] Specifically, the partial current density for C_3 formation through the eCORR was roughly 4 times higher than that of the eCO_2RR. The highest C_3 selectivity (FE of ~28%) was achieved using Cu NPs of a size < 100 nm for the eCORR, which presents around a 6-fold increase compared to Cu powders of 5 μm. Further experiments in a flow cell for the eCORR at a constant current density of 300 mA cm^{-2} still present a high 1-propanol FE of 18%. These results demonstrate the new possibility to enhance C_3 selectivity through the combination of Cu NPs and the eCORR.

Despite their great catalytic potential, CuNPs may suffer from inevitable structural reconstruction, which can alter the initial morphology and active sites. Either precise control over catalyst reconstruction or suppression of such reconstruction through rational nanostructure design is therefore highly desirable. For instance, the Yang group has proposed an ensemble catalyst derived from well-assembled Cu NPs for selective eCO_2RR to C_2–C_3 products at low overpotentials[66] (Fig. 3a) and unraveled a dynamic "electrochemical scrambling" mechanism that drove the reconstruction of Cu NPs to disordered Cu nanocrystals through systematic ex situ, passivated ex situ and in situ characterization.[67] The electrochemically scrambled Cu nanocrystal was probed as the critical component leading to enhanced selectivity towards C_2–C_3 products. Note that although this type of catalyst facilitated overall C–C coupling, the enhancement in C_3 selectivity was not as profound as that of C_2. More precise manipulation of the reconstruction process therefore remains valuable to further optimize the yields of higher-carbon products beyond those of C_2. Alternatively, the reconstruction can be suppressed by the design of robust nanostructured Cu catalysts. For instance, Zhao et al. developed a facile surfactant-free synthesis method to obtain Cu_2O nanocrystals with various architectures, which can be further transformed into Cu catalysts under eCORR conditions without much change in the morphology (Fig. 3b).[68]

Among all the directed architectures, the catalyst with a morphology of a branching cubic framework (BCF-Cu_2O) exhibited fivefold higher partial current density of 1-propanol at −0.45 V vs. RHE than the surfactant-coated nanocube catalyst. According to DFT calculations, the clean surface and the exposure of Cu(100) and Cu(110) were found to facilitate 1-propanol production, which corroborated with the high catalytic activity of BCF-Cu_2O exhibiting the highest exposure of Cu(100) and Cu(110) facets. In addition to the sophisticated engineering of synthesis procedures, the adoption of a support to anchor the nanoparticles presents another possibility to stabilize the Cu nanostructure. According to Lu et al., dispersing Cu/Cu_2O nanoparticles on nitrogen-doped graphene enabled nearly a one-fold increase in the 1-propanol FE during the eCO_2RR.[69] In brief, all above studies highlight the importance of morphology control for Cu catalysts in enhancing C_3 formation.

In addition to regulating the characteristics and densities of active sites, micro-/nanostructure engineering on Cu catalysts can also tune the concentration and coverage of key reaction intermediates such as C_2 and CO. For instance, studies on porous or hollow-structured catalysts have demonstrated the effectiveness of exploiting the confinement effect to steer the selectivity from C_1 to C_{2+}.[71,72] This idea can be further leveraged to increase C_3 yields. Sargent et al. developed a methodology to synthesize open Cu nanocavities and adjust their geometry by varying the acid-etching time of Cu_2O pre-catalysts.[73] The finite-element method (FEM) was adopted to verify the restricted diffusion of locally produced C_2 species in the cavity, a higher concentration of which was found to be responsible for increasing its probability to couple with CO, leading to a higher C_3 production rate. With an optimized Cu nanocavity, the FE of 1-propanol from the eCORR can reach a maximum of 21 ± 1% at a conversion rate of 7.8 ± 0.5 mA cm^{-2}. Alternatively, Zeng et al. leveraged a different synthetic method based on Ostwald ripening and fabricated a series of Cu_2O hollow multi-shell structures (HoMSs) with tunable shell numbers (Fig. 3c). They demonstrated that the 3-shell HoMSs with a stronger nano-confinement effect exhibited a sharp increase of 1-propanol FE from negligible (1-shell HoMSs) and <2% (2-shell HoMSs) to >15% (at −0.65 V vs. RHE).[70] Similar effects of multi-shell structures on promoting C_3 formation were also demonstrated with the eCORR.[74] These studies showcase rational micro-/nanostructuring as a promising physical route, in addition to the conventional active site regulation approach, to steer the product selectivity towards C_3 products during the eCO_2RR and eCORR.

2.3.2. Defect engineering. While the aforementioned efforts can be summarized as a "bottom-up" strategy to engineer the micro-/nanostructure of Cu-based catalysts, there also exists a "top-down" strategy that has been leveraged more frequently in eCO_2RR research.[48,51,75–79] For instance, OD-Cu type materials, usually resulting from electroreduction of Cu (hydro) oxide pre-catalysts (e.g. CuO, Cu_2O, and $Cu(OH)_2$), contain enriched structural defects such as grain boundaries. Adopting the $Cu_2O/Cu(OH)_2$ film as a precursor for preparing defect-rich Cu catalysts, Yeo et al. estimated the population of defects using cyclic voltammetry and then established a linear correlation

19668 | J. Mater. Chem. A, 2024, **12**, 19663–19684

This journal is © The Royal Society of Chemistry 2024
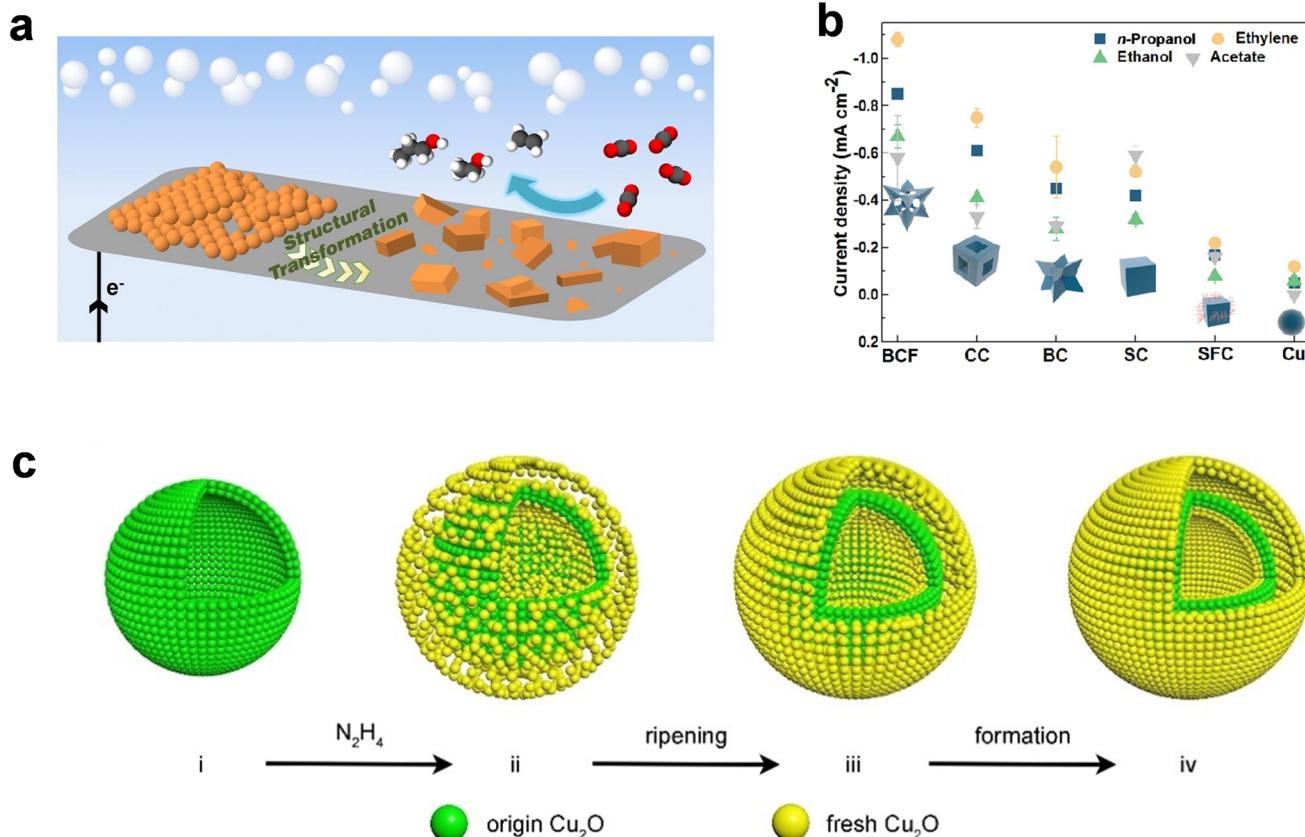
Fig. 3 Micro-/nanostructure engineering of Cu-based catalysts. (a) Schematic illustration of the transformation process of Cu NP ensembles into an active catalyst for C_3 product formation. Adapted from ref. 66 with permission from National Academy of Sciences. (b) Partial current density of 1-propanol through the eCORR on a variety of catalysts derived from surfactant-free Cu_2O nanocrystals at -0.45 V vs. RHE. Adapted from ref. 68 with permission from American Chemical Society. (c) Schematic illustration of Cu_2O HoMSs with different numbers of layers. Adapted from ref. 70 with permission from Wiley-VCH GmbH.

between the defect population and the yield of 1-propanol.[48] This work highlights the role of defects in stabilizing key intermediates for C–C coupling, which are presumably CO* and C_2H_4 precursors. The type of defect in OD-Cu that correlates with C_3 production was further investigated. Since the Cu(111) and Cu(100) facets have been proved to be C_1-selective and C_2-selective, respectively,[46,80,81] the boundary between these two facets was hypothesized as the C_3-specific sites in OD-Cu. Along this line, Sinton et al. synthesized high-fragmented copper (HF-Cu) by controlling the crystalline domains of CuO pre-catalysts (Fig. 4a).[51] The HF-Cu catalyst was shown to contain the largest density of fragments consisting of adjacent Cu(100) and Cu(111) facets. With other possible effects brought by Cu atomic environments (oxidation states, coordination, or strain) ruled out through comprehensive characterization, the Cu(100)/Cu(111) interface per area, measured from the high-resolution transmission electron microscopy images, was found to linearly correlate with the 1-propanol FE (Fig. 4b). The promotion of C_1–C_2 cross-coupling by the Cu(100)/Cu(111) interface was also rationalized by the lowered coupling barrier from DFT calculations. However, the grain boundaries were also identified to promote other products such as acetate and methane.[82] Thus, the specificity of the grain boundary in promoting C_3 products

requires further investigation and the precise modulation of desirable grain boundaries presents a promising direction in future research.

Besides grain boundaries, other types of defects in OD-Cu or other Cu catalysts derived from compound pre-catalysts can also efficiently promote C_3 formation. Shown as under-coordinated protuberances on ordinary crystal planes, Cu adparticles were proved by DFT calculations to be excellent site motifs to enhance the chemisorption of CO as well as its coupling with C_2 surface species such as OCCOH* and CCH_2^*.[76] Further manipulating the reconstruction of an OD-Cu catalyst in a CO-enriched environment allowed for the creation of an adparticle structure, which achieved an exceptional FE of 23% for 1-propanol, surpassing that of OD-Cu only rich in grain boundaries with no adparticles. The density of under-coordinated sites can be regulated by not only a gas atmosphere but also OD-Cu precursors. For instance, Gong et al. systematically compared different precursors (i.e. Cu_2O, CuO, and $Cu(OH)_2$) of OD-Cu and found that OD-Cu from $Cu(OH)_2$ possessed a relatively high density of stepped Cu(110) and Cu(100), which allowed for higher CO coverage and more facile CO–CO coupling, respectively. The highest FE of $\sim$11% for 1-propanol (at -0.98 V vs. RHE) can be consequently achieved

This journal is © The Royal Society of Chemistry 2024

J. Mater. Chem. A, 2024, 12, 19663–19684 | 19669
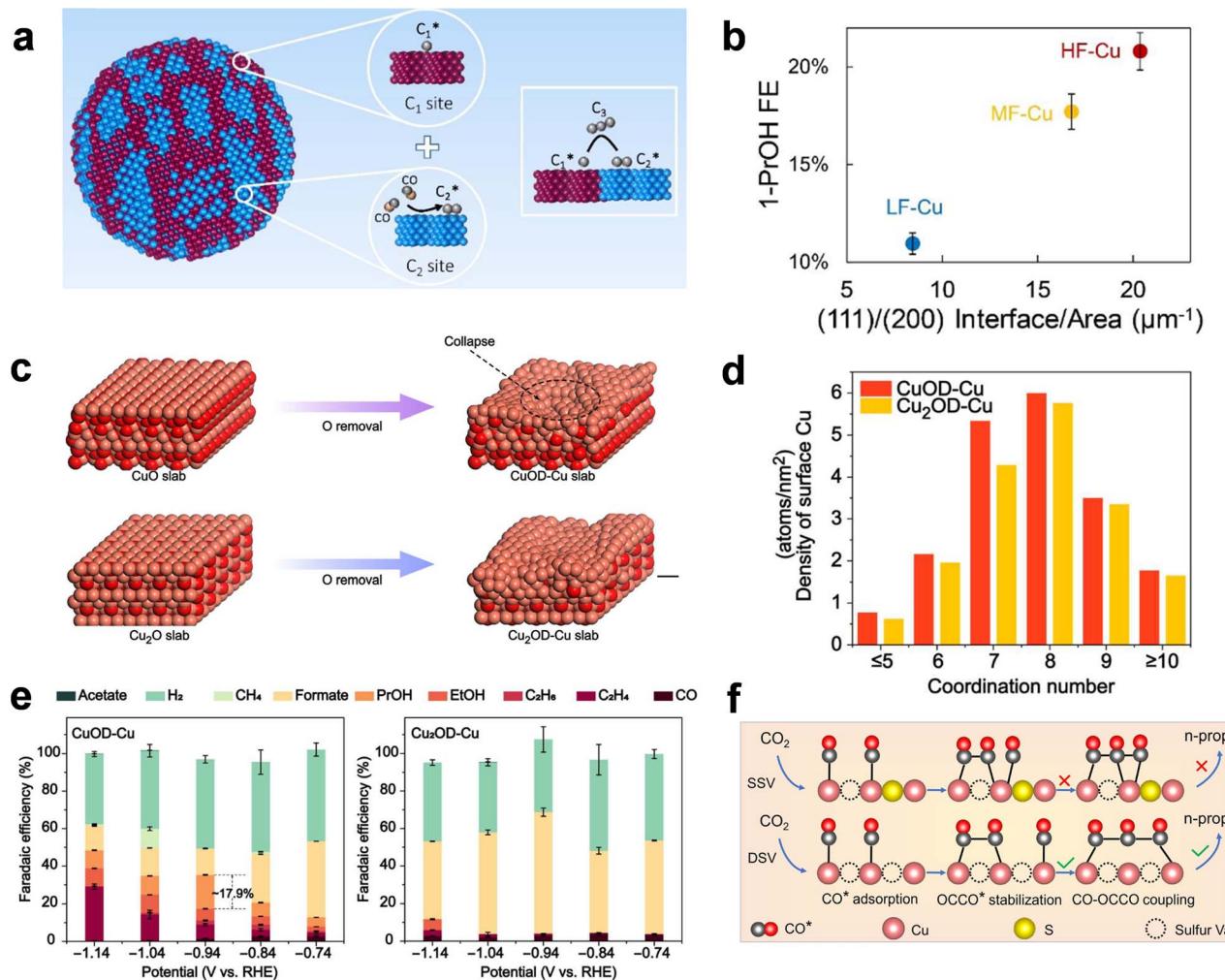
Fig. 4 Defect engineering of Cu-based catalysts. (a) Schematic illustration of HF-Cu with enriched (100)/(111) grain boundaries. (b) The Cu(111):(100) interface per area, measured from the high-resolution transmission electron microscopy images, plotted against the 1-propanol selectivity performance. Adapted from ref. 51 with permission from Springer Nature. (c) Simulated initial models and final configurations after oxygen removal (from CuO to CuOD-Cu and from Cu_2O to Cu_2OD-Cu) using neural network potential-based molecular dynamics simulation. (d) Coordination number dependent surface Cu density on CuOD-Cu and Cu_2OD-Cu. (e) FE of products on CuOD-Cu (left) and Cu_2OD-Cu (right) during the eCO_2RR in a H-cell. Adapted from ref. 83 with permission from American Association for the Advancement of Science. (f) Schematic illustration of the 1-propanol formation mechanism on adjacent CuS_x-DSV. Adapted from ref. 75 with permission from Springer Nature.

among the three types of OD-Cu.[77] Leveraging neural network potential based molecular dynamics and *in situ* X-ray absorption spectroscopy, Tang *et al.* also demonstrated that OD-Cu from CuO possessed an intrinsically higher population of undercoordinated Cu sites than the counterpart from Cu_2O owing to the vigorous oxygen-removal-induced structural collapse during CuO electroreduction (Fig. 4c and d).[83] The high-density under-coordinated defect sites were suggested to increase the population of CO* and *HOCCOH intermediates by both *in situ* spectroscopy and computational simulations, leading to a promising FE of 17.9% for 1-propanol at −0.94 V *vs.* RHE (Fig. 4e). The reconstruction process can be further regulated by decorating CuO with Au NPs, which aided the formation of more disordered Cu structures and resulted in a record high 1-propanol FE of 46.6% obtained in a flow cell.[78]

In contrast to the "protuberant" under-coordinated defect sites out of a standard crystal facet, vacancies can be deemed as a "dented" counterpart by removing either cationic or anionic atoms and leaving holes on the surfaces. Sargent *et al.* reported that the modification of the Cu_2S core with Cu surface vacancies led to an impressive FE of $8 \pm 0.7\%$ for 1-propanol production, but it was also notable that the Cu vacancies were not only selective to 1-propanol but also ethanol.[79] An alternative strategy to selectively enhance 1-propanol production over other alcohols is to precisely generate double sulfur vacancies (DSVs) on CuS using a controllable lithium electrochemical tuning method.[75] As demonstrated by Zheng *et al.*, DSV-rich CuS_x catalysts, obtained after 10 charge/discharge cycles in a lithium electrochemical cell, exhibited the highest FE of 15.4% for 1-propanol; whereas neither decreasing nor increasing the cycle

19670 | *J. Mater. Chem. A*, 2024, **12**, 19663–19684

This journal is © The Royal Society of Chemistry 2024

numbers gave rise to better yields of 1-propanol, highlighting the pivotal role of DSV that possessed an optimized Cu–Cu distance in facilitating CO trimerization (Fig. 4f). Similar to the observations on grain boundaries, defect sites such as vacancies, albeit enabling an increase in C_3 selectivity in some cases, require delicate structural control to realize the C_3-specific eCO$_2$RR. The structure–property relationships are so far case-specific, and somewhat lack generality. The synthetic methods to manipulate the types and population of, if C_3-specific, certain active defect sites also diverge.

2.3.3. Oxidation state regulation. Other than the defect generation during *in situ* transformation of OD-Cu, there exists another perspective to rationalize the enhanced C_{2+} formation on OD-Cu, that is, the regulation of oxidation states and consequently the electronic structure of Cu sites induced by residual oxygen.[84–89] While a large body of existing studies have revealed the key role of polarized $Cu^{\delta+}$ ($0 < \delta \leq 1$) sites,[84,85,88] as well as the interface between Cu^0 and Cu^+ phases,[86,87] in facilitating C–C coupling, only a few studies attempted to tie the oxidation states of Cu with C_{3+} formation. For example, Lee *et al.* observed C_3–C_4 production during the eCO$_2$RR for a limited duration and suggested a metastable bi-phasic Cu_2O–Cu surface accounting for such an activity.[90] Cuenya *et al.* compared Cu nanocube catalysts with different plasma pretreatments and found that O_2 plasma induced the highest initial oxygen content and led to the highest FE of 9% for 1-propanol despite the reduced surface roughness. Though presenting great catalytic potential, the long-term stabilization of $Cu^{\delta+}$ sites under reductive conditions, however, remains a challenge.[91] Because of the enormous thermodynamic driving force of reducing $Cu^{\delta+}$ to Cu^0 within the voltage window of the eCO$_2$RR, the dynamics of the reducing process could play a vital role in securing the stable presence of $Cu^{\delta+}$ active sites. By applying pulsed electrolysis programs in which anodic and cathodic potentials were alternately sequenced, desirable defects and Cu^+ species were *in situ* generated to favor the continuous eCO$_2$RR with high C_{2+} selectivity.[85] It was found that the parameters for pulsed electrolysis, such as the values of anodic potential[85] and the pulsed intervals,[86] exhibited strong impacts on the product selectivity. A moderate anodic potential of 0.6 V *vs.* RHE and a narrow range of cathodic/anodic pulse durations allowed for an optimized dynamic balance between oxidized and reduced Cu species. The above experimental observation can be further rationalized by neural-network-potential-based, large-scale molecular dynamics of OD-Cu reconstruction.[92] As demonstrated by Lian *et al.*, while it is true that OD-Cu would be fully reduced to metallic Cu after long-term electrolysis, agreeing well with the reduction thermodynamics, the dynamics of removing all trapped oxygen were actually slow. Therefore, this work lays a theoretical foundation for the dynamic stabilization of $Cu^{\delta+}$ sites in pulsed experiments. Other effects such as the Mott–Schottky effect were also leveraged to stabilize $Cu^{\delta+}$ sites.[93] Nevertheless, similar to structural defects, the specificity of positively charged Cu sites, if necessarily stabilized in the catalytic phases, to C_3 products as opposed to other multicarbon products such as C_2 still remains elusive.

2.3.4. Foreign element regulation. The introduction of foreign atoms into Cu, such as by alloying and doping, is considered as another effective way to modulate the active sites of Cu-based catalysts. The foreign element either offers additional sites to enable pathways that are unfavorable on pristine Cu, or to regulate the coordination environment as well as the electronic structure of adjacent Cu sites. As the generation of C_3 products relies on successive C_1–C_1 coupling and C_1–C_2 coupling where CO presents the most likely C_1 precursor, it is essential for the catalytic surface to simultaneously provide moderate CO binding and increase CO coverage. Therefore, the addition of a second elemental component capable of producing CO selectively presents a viable route to facilitate C–C coupling on Cu-based surfaces.[94] Elemental candidates to achieve more selective CO production than Cu include Zn, Ag, Au, and Pd.[95] Although Cu-based alloys consisting of these metals have been widely reported for the eCO$_2$RR/eCORR towards C_{2+} products,[96–100] the specific improvement of C_3 selectivity can be realized by further engineering. And the mechanisms of favoring C_3 production over other C_{2+} chemicals vary with the identity of foreign elements, as well as their concentration.

Manipulating the phase segregation of initial alloys could be a useful strategy to isolate CO formation and C–C coupling on different domains. For instance, Broekmann *et al.* prepared a binary CuPd alloy with a nominal composition of $Cu_{91}Pd_9$ and further adopted a sequential treatment of air annealing and *in situ* reduction to induce phase segregation, which resulted in Pd-rich and Cu-rich domains, respectively (Fig. 5a).[101] While the Pd-rich domains promoted CO formation during the eCO$_2$RR, CO was then transported to the Cu-rich ones for subsequent C–C coupling. The increased CO availability induced by Pd-rich domains led to higher propensity of C–C coupling. Interestingly, the seminal work by Kenis *et al.* unraveled the key role of phase segregation in generating more C_2 than C_1 chemicals during the eCO$_2$RR.[97] The distinctive product distributions of phase-separated CuPd alloy systems in the above two studies can be rationalized through the different ratios of Pd : Cu. While the equal-molar system (Cu : Pd = 1 : 1) primarily facilitates C_2 products such as ethylene (FE > 40% at −0.65 V *vs.* RHE) and ethanol (FE > 14% at −0.65 V *vs.* RHE), as shown by Kenis *et al.*,[97] the work by Broekmann *et al.*[101] showed that decreasing Pd content favored C_3 (FE = 13.7 ± 0.8% at −0.65 V *vs.* RHE) over C_2 products (*e.g.* FE$_{ethanol}$ = 7.1 ± 0.3% at −0.65 V *vs.* RHE).A sSimilar effect by dilute alloying was also demonstrated by Ye *et al.*, who introduced a family of facet-defined dilute CuAu alloy nanorods (NRs) with precisely controlled Au atomic content from *ca.* 1% to 16%.[102] All these NR alloy catalysts possessed uniform crystal shapes with preferentially exposed (100) surfaces, among which the NR2 catalyst with a nominal composition of $Cu_{98}Au_2$ exhibited the highest FE of 18.2 ± 0.3% for 1-propanol at −0.41 V *vs.* RHE (Fig. 5b). Note that NR5 and NR6 with more than 12 at% Au exhibited phase separation, yielding nanocrystalline Au. However, phase separation in this case favored C_1 formation rather than C_3. Therefore, it is pivotal to precisely control both the mixing patterns and content of the

This journal is © The Royal Society of Chemistry 2024

J. Mater. Chem. A, 2024, **12**, 19663–19684 | **19671**
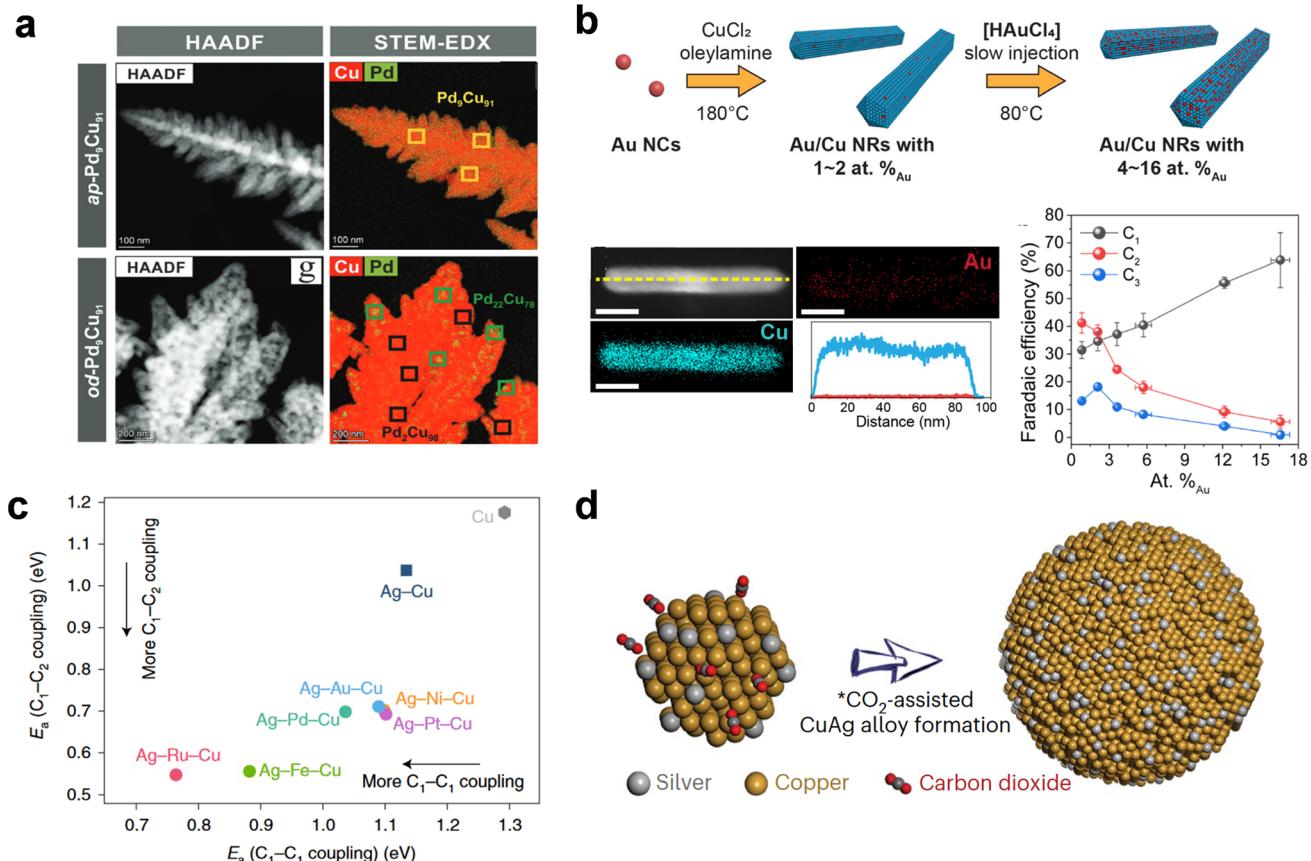
Fig. 5 Foreign element regulation of Cu-based catalysts. (a) Phase segregation from the as-prepared CuPd alloy (ap-Pd_9Cu_{91}) to the activated sample (od-Pd_9Cu_{91}), as revealed by high-angle annular dark-field scanning transmission electron microscopy (HAADF-STEM) and STEM energy-dispersive X-ray spectroscopy (EDS) images. Adapted from ref. 101 with permission from The Royal Society of Chemistry. (b) (Upper) schematic illustration of Au/Cu NR synthesis, (bottom left) HAADF-STEM image and STEM-EDS elemental maps of a single NR with 2.1 ± 0.3 at%$_{Au}$, and (bottom right) FEs of C_1, C_2, and C_3 products vs. the Au contents of NRs. Adapted from ref. 102 with permission from American Chemical Society. (c) DFT-calculated activation energy (E_a) for C_1-C_1 and C_1-C_2 coupling on screened Ag–X–Cu systems (X = Au, Pd, Pt, Ni, Fe and Ru). Adapted from ref. 103 with permission from Springer Nature. (d) Schematic illustration of a supersaturated CO_2-stabilized CuAg alloy with highly dispersed Ag atoms. Adapted from ref. 104 with permission from Springer Nature.

foreign element in the Cu-based alloys for selective eCO$_2$RR towards C$_3$ products.

Compared to the eCO$_2$RR, the eCORR could take advantage of alkaline electrolysis and direct gas feeding. The former enables higher C$_2$ yields than acidic or neutral electrolysis, and the latter leads to better mass transport management. In addition, the absence of a CO$_2$-to-CO pathway in the eCORR allows for better mechanistic understanding of the effect induced by foreign elements on C$_2$/C$_3$ selectivity tuning. Combining Cu-based dilute alloys with the eCORR has been demonstrated to yield significant improvement in C$_3$ selectivity. For example, Sargent et al. theoretically designed an Ag-doped Cu alloy surface with asymmetric C–C coupling active sites, which exhibited the lowest activation barriers for both C$_1$–C$_1$ and C$_1$–C$_2$ coupling to form C$_3$ products among various single metal (i.e. Ag, Au, Ru, Rh, and Pd) doped Cu surfaces.[105] Such a design was experimentally realized using a dilute Cu$_{96}$Ag$_4$ alloy for the eCORR in a flow cell reactor with a GDE, which exhibited a promising FE of 33 ± 1% for 1-propanol at -0.46 V vs. RHE (in 1 M KOH solution). The FE towards 1-propanol can be further

enhanced to 37 ± 3% at a high current density of 300 mA cm^{-2} in a MEA-based reactor, by introducing only 1 at% of Ru to the dilute Ag-in-Cu system.[103] The theoretical calculations further revealed that the additional isolated Ru dopant can induce higher coverage of CO* and lower activation barriers for both C$_1$–C$_1$ and C$_1$–C$_2$ coupling (Fig. 5c). Alternatively, the specific CuAg system for alkaline eCORR can be engineered by altering the precursor from pure Cu to Cu compounds. Fontecave et al. investigated a series of catalysts derived from metal-doped Cu nitrides (denoted as CuM$_{x\%}$N$_{t\ h}$ with x giving the mol% of the doping metal M and t the time for nitridation), among which CuAg$_{5\%}$N$_{20\ h}$ showed an optimized FE of 45% for 1-propanol at 150 mA cm^{-2}.[106] The higher C$_3$ selectivity of CuAg$_{5\%}$N$_{20\ h}$ compared to CuAg$_{5\%}$ was attributed to increased roughness and porosity, while the introduction of Ag, consistent with other reports, was reported to lower C$_1$–C$_2$ coupling barriers.

Interestingly, the product distributions within the dilute bimetallic CuAg systems that deliver the most promising C$_3$ selectivity are still highly tunable by regulating the reaction conditions and local environments. For example, in the above

19672 | J. Mater. Chem. A, 2024, **12**, 19663–19684

This journal is © The Royal Society of Chemistry 2024

work by Fontecave *et al.*, systematic investigations were performed to unravel the effect of the CO feeding rate and electrolyte properties.[106] Key findings include that (1) a moderate CO feeding rate enables a delicate balance between surface-adsorbed CO* and C_2 intermediates inclined to coupling, which corroborates well with the competitive co-adsorption study of CO and acetaldehyde by Koper *et al.*;[107] (2) the formation of 1-propanol exhibits an exceptional interfacial electric field effect, which becomes profound on increasing the concentration of cations or changing the cation from K^+ to Cs^+; (3) a too-high alkaline concentration is detrimental to 1-propanol production due to the reaction pathway bifurcation to acetate,[42] which offsets the advantage of the cation-induced field effect at high concentrations. The regulation of reaction environments can even alter the identity of major C_3 products. Adopting CO_2-supersaturated conditions, Voiry *et al.* reported the electrosynthesis of a rarely observed C_3 product, 2-propanol, from the eCO_2RR on a $Cu_{94}Ag_6$ alloy catalyst with a high FE of 56.7% at -0.70 V *vs.* RHE (in 1 M $CsHCO_3$ solution with $\sim$3 M CO_2).[104] The CO_2-supersaturated condition was found to provide combinatorial effects by suppressing the phase segregation and modulating CO* adsorption strength/coverage (Fig. 5d). The resultant highly dispersed Ag atoms in Cu weakened the surface–O binding and thus protected the secondary C–O bond from cleavage, leading to favorable formation of 2-propanol over 1-propanol. This mechanism is possibly dominated by the ligand effect of Ag, as evidenced by the charge transfer between Ag and Cu.

In addition to the ligand effect, the doping atom could induce a strain effect through atomic size misfitting. Zhang *et al.* reported that doping Pb ($\sim$2.9 at%), an extremely heavy element with a large atomic radius, in Cu resulted in numerous atomic Pb-concentrated grain boundaries and induced a large number of under-coordinated Cu sites after geometric structural distortion.[108] The FE of CO-to-1-propanol can consequently reach $47 \pm 3\%$ at -0.68 V *vs.* RHE. Note that Pb is classified as a formate-producing rather than CO-producing element in the eCO_2RR. This work clearly showcased an approach of regulating Cu with an "inactive" foreign element, distinctive from designing Cu-based alloys with CO-active elements.

Despite the great potential of dilute Cu-based alloys for selective $eCO_2RR/eCORR$ to C_3, it should be noted that due to the complexity in reaction pathways and sensitivity of key steps to reaction conditions/environments, the operational window for attaining desirable selectivity is rather narrow. Thus, combinatorial investigation is advocated in future research when focusing on complex products like C_3.

2.3.5. Single-site Cu catalysts. Single-site Cu catalysts present a unique class of Cu-based catalysts with atomic Cu embedded in a solid substrate (usually carbon), coordinated frameworks, or macrocyclic molecules. The site geometry places an upper limit for the maximum number of adsorbates (*i.e.* usually one), and thus the products of the $eCO_2RR/eCORR$ on such types of catalysts are limited to C_1 products in most cases. However, Chen *et al.* reported the observation of acetone as a major product during the eCO_2RR on single-atom Cu encapsulated on nitrogen-doped porous carbon (Cu-SA/NPC).[109] The

highest FE for acetone was obtained as 36.7% at -0.36 V *vs.* RHE. Systematic control experiments and theoretical calculations confirmed that both the single-site Cu and surrounding pyrrolic-N remained crucial to acetone formation and that changing the coordination atoms from pyrrolic-N to pyridinic-N hindered efficient CO–CO coupling. While it is interesting that coordination N atoms can participate in chemical bonding and break the single-metal-site geometric limitation to multiple chemisorptions, there are other studies discussing the reconstruction of single-site Cu catalysts to Cu clusters or nanoparticles, in which the *in situ* formed Cu multisite ensembles were believed to account for the C_{2+} formation.[110,111] Therefore, the ability of single-site Cu catalysts for selective C_3 formation requires further investigations with the assistance of *in situ* structural and surface-state characterization studies.

2.4. Non-Cu catalysts

Cu-based catalysts, though yielding impressive FEs towards C_{3+} products, still require rather large overpotentials to achieve satisfactory production rates. And the vast possibilities in coupling routes also make the selectivity control of Cu-based catalysts challenging. The suitable operational window for Cu-based materials to selectively catalyze C_3 formation largely hinges on the type of reactors, the carbon source (*e.g.* CO_2, CO, or their mixtures), and the electrolyte. One reason for such sensitivity could be attributed to the highly polar nature of key intermediates such as CO_2^* and its protonated forms, the CO dimer, as well as other carbonyl compounds. These polar intermediates are prone to complex interfacial effects from the solvent, ion, and electric field. Thus, the journey to search for non-Cu-based catalysts with lower overpotentials or alternative C–C coupling mechanisms never ceases.

Promising substitutes for Cu include various metal compounds such as molybdenum (Mo)-based and nickel (Ni)-based materials. The original pure metallic Mo and Ni exhibit much stronger CO* adsorption than Cu and present negligible eCO_2RR activity due to the severe CO poisoning and undesirable reaction energetics of CO protonation or CO–CO coupling. Their compounds with nonmetal elements, however, have generally weaker binding due to the more filled metal d-states, thereby exhibiting potential catalytic capability of interest. For instance, Lewis *et al.* observed 1-propanol to be the major eCO_2RR product on single-crystal or thin-film MoS_2 electrodes, although the maximum FE ($\sim$3.5%) was far below that of the competing hydrogen evolution reaction (HER, FE of $\sim$50–60%).[112] They also revealed the active sites for the eCO_2RR to 1-propanol to be MoS_2 terraces rather than its edges. Despite the substantial HER activity and self-decomposition, MoS_2 indeed demonstrates unique eCO_2RR properties compared with Cu. Understanding the origin of such unique eCO_2RR activity would be valuable for guiding the design of non-Cu catalysts.

Other than MoS_2, Ni-based catalysts present another group of promising candidates to yield higher-order products from the eCO_2RR. In the seminal work by Paris and Bocarsly, Ni_3Al alloy films on glassy carbon electrodes have been demonstrated to produce 1-propanol (FE = $1.9 \pm 0.3\%$) in addition to

This journal is © The Royal Society of Chemistry 2024

J. Mater. Chem. A, 2024, **12**, 19663–19684 | **19673**

a substantial FE (~30%) of forming CO.[113] Their subsequent work further pointed out the necessity of the intermetallic character at the atomic scale to provide distinct yet complementary sites for the eCO$_2$RR to 1-propanol.[114] The investigation of the H/D isotope effect also suggested a reaction mechanism different from that on Cu. Combining theory and the experiment, Yeo *et al.* achieved success in stabilizing the polarized Ni$^{\delta+}$ active sites, which exhibited moderate CO binding and generated a variety of mixed long-chain C$_3$–C$_6$ hydrocarbons with a total FE of up to 6.5% in the electrolyte of 0.1 M KHCO$_3$.[115] In contrast, metallic Ni remained inactive. In addition, the authors proposed a novel reaction mechanism reminiscent of the Fischer–Tropsch synthesis: COOH + CH$_x$ coupling followed by successive CH$_x$ insertions, which remains rather distinctive from CO–C$_2$ coupling or even CO trimerization on other catalysts (Fig. 6a). This mechanism was further validated through the invariant C$_{3+}$ yield with the addition of CO or formaldehyde (CH$_2$O) feedstock.

Similarly, new reaction mechanisms have also been proposed on nickel phosphides (Ni$_x$P$_y$). For instance, Dismukes *et al.* verified the capability of P-rich Ni$_x$P$_y$ (Ni$_{12}$P$_5$, Ni$_2$P, Ni$_5$P$_4$, and NiP$_2$) to convert CO$_2$ to C$_3$ (methylglyoxal) and C$_4$ (2,3-furandiol) products at a very low overpotential (<50 mV) with high selectivity (maximum FE = 84% for C$_3$ on NiP$_2$ at −0.1 V *vs.* RHE; maximum FE = 71% for C$_4$ on Ni$_2$P at 0 V *vs.* RHE), successfully simulating the catalytic performance of Ni-based enzymes.[116] In addition, the authors suggested a reaction mechanism radically different from that of Cu; formation of formate as the oxygenated precursor happens first, followed by the formation of CH$_2$O, and self-condensation of CH$_2$O

(Fig. 6b). Rappe *et al.* further adopted DFT calculations to investigate such a mechanism on Ni$_2$P, revealing that the rate-determining step was surface hydride transfer to physisorbed CO$_2$, a non-electrochemical step.[117] Therefore, simultaneous engineering of both thermal and electrochemical steps remains a valuable strategy to further optimize Ni$_x$P$_y$-based catalysts.

According to the above studies, it is evident that the reaction steps on non-Cu catalysts are significantly different from the ones reported on Cu-based systems. The precursors for C–C coupling vary from CO (for the majority of Cu-based materials) to hydrocarbons and formate (for non-Cu catalysts). Consequently, more comprehensive understanding of the specific reaction mechanism remains extremely vital to ensure rational design of future catalysts with enhanced catalytic activity and selectivity towards C$_{3+}$ products. Another challenge and opportunity lies in the suppression of the HER side reaction. A Mo- and Ni-based compound catalyst, albeit with decent C$_{3+}$ selectivity in eCO$_2$RR products, normally suffer from severe HER competition. The most promising C$_{3+}$ activity and selectivity are mainly observed at low overpotential and low current density. In fact, at higher overpotential where industrially desired current density is achievable, most metal sulfides and phosphides were found to be predominantly active towards the HER rather than the eCO$_2$RR.[118] Seeking for compatible HER-suppression strategies might offer opportunities to fully exert the catalytic properties of non-Cu catalysts. In this sense, Asadi *et al.* reported imidazolium-functionalized Mo$_3$P NPs with an ionomer coating for selective eCO$_2$RR to propane.[119] Both the imidazolium functionalization and ionomer coating created a relatively hydrophobic environment and increased the
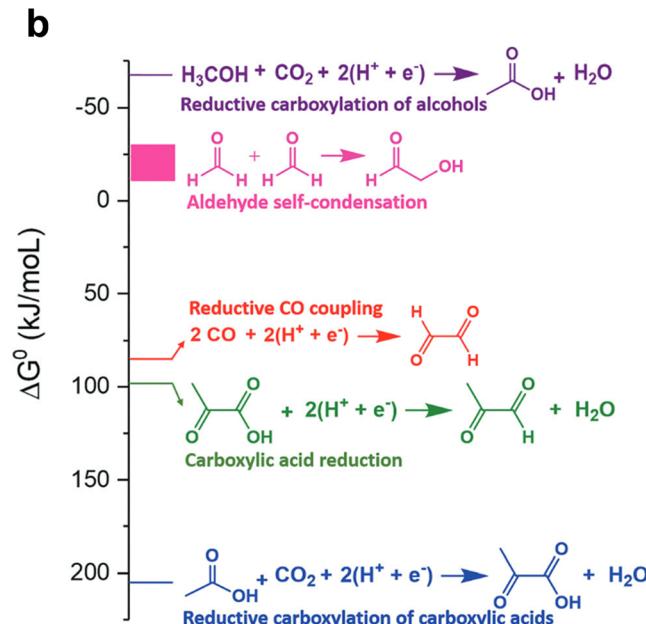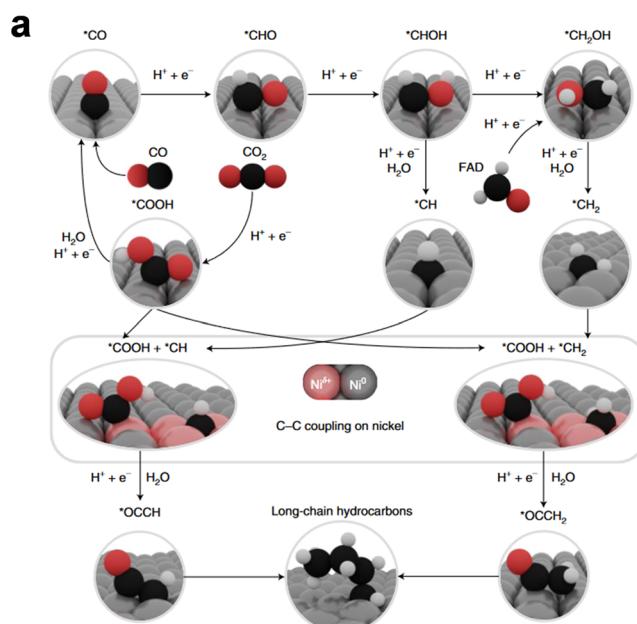
Fig. 6 Non-Cu catalysts. (a) Initial steps in the C−C coupling towards long-chain hydrocarbons on polarized Ni sites. The insertion mechanism, schematically depicted at the bottom of the figure, is expected to sustain the production of C$_{3+}$ products. Adapted from ref. 115 with permission from Springer Nature. (b) Standard Gibbs free energy changes of possible C−C bond forming reactions (298 K and pH 7), supporting the formaldehyde condensation mechanism on Ni$_x$P$_y$ catalysts at near-thermoneutral potentials. Adapted from ref. 116 with permission from The Royal Society of Chemistry.

19674 | *J. Mater. Chem. A*, 2024, **12**, 19663–19684

This journal is © The Royal Society of Chemistry 2024

CO_2/water ratio near the catalytic surface, resulting in suppressed HER. The positively charged imidazolium further modified the interfacial electric field and adsorption energies of carbon-based intermediates on Mo atoms, directing to a propane-formation pathway in which the trimerization was initiated from co-adsorption of CO* + CH* + CO*. Thanks to the synergistic effects between Mo_3P, imidazolium, and ionomer coating, a promising FE of 91% for propane was obtained at −0.8 V vs. RHE, demonstrating the great potential of non-Cu catalysts for C_3 electrosynthesis from CO_2/CO with desirable selectivity/activity after rational catalyst-reaction microenvironment co-design.

3. "Electrochemical + X" approaches

Direct electrochemical approaches for converting CO_2 to C_{3+} chemicals have seen significant progress in novel catalyst development and industrially applicable reactor design. C_3 molecules such as 1-propanol have been reported as the primary product from direct electrocatalysis.[66,68] While the success of generating species beyond C_3 has been established in a few cases mostly with non-Cu catalysts having distinctive reaction mechanisms,[115,116] the production of C_4 molecules such as 1-butanol ($CH_3CH_2CH_2CH_2OH$) has rarely been reported to occur with measurable quantities through a single electrochemical process. Although studies have suggested that minor and yet-to-be-quantified amounts of 1-butanol can be produced through the eCO_2RR[120] or co-electroreduction of acetaldehyde and CO on OD-Cu electrodes,[59] the extremely low selectivity makes these processes impractical for direct C_4 production. More importantly, a greater gap exists between the products from direct eCO_2RR and desirable C_{5+} target chemicals, such as synthetic gasoline ($C_4–C_{12}$), sustainable aviation fuels ($C_8–C_{16}$), aromatics (C_{6+}), and life-related organic chemicals including saccharides, amino acids, and lipids. Electrochemical upgrading of CO_2 towards more complex chemicals therefore requires complementary processes to leverage eCO_2RR-attainable chemicals for advanced synthesis in tandem.

3.1. "Electrochemical + homogeneous reaction" approaches

Before the discussion on coupling different processes, it is prerequisite to reveal the C_4 formation mechanism on the most investigated Cu-based catalysts. In this regard, Yeo et al. conducted systematic eCO_2RR experiments on OD-Cu in a GDE-based flow cell.[121] By improving the detection and quantification of liquid products with low FEs through a flow cell and headspace gas chromatography, they did observe the formation of 1-butanol in alkaline electrolyte, but the FE was as low as 0.056% and the partial current density was only 0.080 mA cm^{-2}. Unlike the formation of C_3 species that usually involves one individual C_1 adsorbate (e.g. *CO), the aldol condensation of two acetaldehyde molecules was found to account for C–C bond formation, yielding an initial formation of 3-hydroxybutanal ($CH_3CH(OH)CH_2CHO$) (Fig. 7a). The subsequent dehydration then produces crotonaldehyde ($CH_3CH=CHCHO$) as a critical C_4 intermediate, the further $2e^-$-reduced products of which could either be crotyl alcohol ($CH_2CH=CHCH_2OH$) or butanal ($CH_3CH_2CH_2CHO$). Parallel electrolysis experiments of acetaldehyde, crotonaldehyde, crotyl alcohol, and butanal confirmed that the synthetic route towards 1-butanol followed the sequence of acetaldehyde → crotonaldehyde → butanal → 1-butanol while crotyl alcohol remained electrochemically inert. This mechanism was supported by DFT calculations, as well as the promotion of aldol condensation by hydroxide ions (OH^-) and dehydration of 3-hydroxybutanal on Cu surfaces. Collectively, such a mechanism can well explain the low selectivity of C_4 products on Cu during the eCO_2RR or eCORR: (1) the low selectivity towards acetaldehyde on Cu; (2) the competition between acetaldehyde electroreduction to ethanol and aldol condensation; and (3) the hydration of crotonaldehyde to an unreactive form in alkaline solution. Overcoming the above limitations could be realized through a cascade reaction
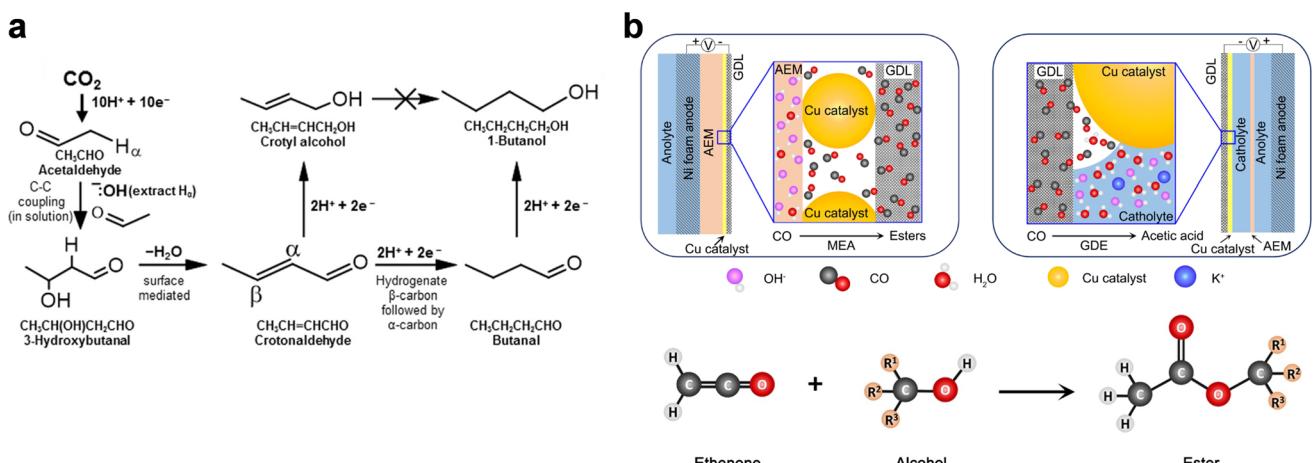
Fig. 7 "Electrochemical + homogeneous reaction" approaches. (a) Simplified domino reaction mechanism for the eCO_2RR to 1-butanol. Adapted from ref. 121 with permission from Wiley-VCH GmbH. (b) Schematic illustration of (upper) the eCORR process in the cathodic compartment of a MEA cell and a GDE embedded in a flow cell, and (bottom) ester formation from the reaction between ethenone and alcohol. Adapted from ref. 122 with permission from Wiley-VCH GmbH.

This journal is © The Royal Society of Chemistry 2024

J. Mater. Chem. A, 2024, 12, 19663–19684 | 19675

engineering approach, where CO_2-to-acetaldehyde conversion, aldol condensation, and crotonaldehyde electroreduction are optimized separately. Such a design might be worthy of future investigations.

In line with the above mechanistic study, it is fundamentally feasible to couple direct electrolysis with controllable homogeneous reactions to steer the product selectivity. Interestingly, Yeo *et al.* demonstrated the production of C_3–C_6 acetate esters through the eCORR in an MEA cell (Fig. 7b).[122] The absence of esters was attributed to the "water-rich" interfacial conditions in conventional H-cells or GDE-based flow cells, which favor the nucleophilic reaction between OH^- and the key intermediate ethenone ($CH_2=C=O$) that leads to acetate production. In the MEA-based eCORR, in contrast, ethenone preferentially reacts with alcohols to yield esters, resulting in an unprecedented total FE of 22% for esters (~20% for ethyl acetate) at 250 mA cm^{-2}. It should be noted that as the major alcohol product during the eCORR was ethanol, the dominant ester product was ethyl acetate (C_4). C_5 and C_6 ester production thus critically relies on the yields of C_3 and C_4 alcohols.

Since the rates of homogeneous reactions remain independent of electrochemical potential, on-site homogeneous reactions can be rate-limiting in the entire integrated process. While introducing catalysts for homogeneous reactions may facilitate the post-eCO$_2$RR transformation, the alignment of different reaction conditions and the separation of homogeneous catalysts from the original eCO$_2$RR systems can be challenging. In addition, the number of homogeneous reactions that can operate under mild ambient conditions is limited. Therefore, we will then move on to discussing the coupling of an electrochemical approach with another type of complementary process, heterogeneous thermocatalytic reactions, in a tandem or cascade manner. Compared to homogeneous reactions, heterogeneous thermocatalytic reactions are more common in industrial manufacture of bulk chemicals and thus offer greater opportunities for process coupling.

3.2. "Electrochemical + thermochemical" approaches

The dependence on fossil-fuel-derived feedstocks (*e.g.* H_2 production *via* extremely energy-consuming steam reforming) in a conventional thermochemical approach for chemical manufacture usually results in positive net CO_2 emissions.[123] Switching from fossil fuels to renewable feedstocks, such as CO, hydrocarbons, and oxygenates derived from direct electrochemical CO_2 reduction, could then potentially offer an alternative to alleviate CO_2 emissions in the conventional chemical industry. The coupling of the eCO$_2$RR with downstream thermochemical synthesis, namely the "electrochemical + thermochemical" approach, seems to be simple and straightforward. However, the separation of required feedstocks from a mixture of products derived from the eCO$_2$RR can be energetically demanding. Integrating a separation unit between the electrochemical and thermochemical modules may offset the advantage of reducing CO_2 emissions but remains necessary in some cases to optimize the reaction conditions of thermochemical reactors. For instance, Wang *et al.* demonstrated that simply inserting a CO_2-absorption procedure between an eCO$_2$RR reactor and a cascade C_2H_4 oxidation reactor can double the production rate of ethylene glycol.[124]

To make the entire process more economically favorable, it is of course more desirable to leverage the mixed products as feedstocks directly for thermochemical conversion without further purification. Reactions requiring mixed reactants therefore naturally emerge as suitable candidates. Due to the ubiquity of CO as the most common product of the eCO$_2$RR, various efforts have been reported to integrate carbonylation reactions in the tandem process. For instance, Chen *et al.* proposed a two-step tandem electrochemical-thermochemical approach to synthesize value-added C_3 oxygenate molecules from CO_2 (Fig. 8a),[125] in which CO_2 was first electrochemically reduced to mixed gas products of C_2H_4, CO, and H_2 on Cu with a MEA reactor. Due to the low solubility of these gas products in aqueous solution, it is convenient to separate them from other liquid products. A thermochemical hydroformylation reaction was then employed to produce propanal ($C_2H_4 + CO + H_2 \rightarrow CH_3CH_2CHO$) and 1-propanol ($CH_3CH_2CHO + H_2 \rightarrow CH_3CH_2CH_2OH$) from a mixed C_2H_4/CO/H_2 feedstock (Fig. 8). It was shown that both the Cu-catalyst-dependent gas inlet composition and the reaction temperature can influence C_3 yields and selectivity. The optimized C_3 oxygenate selectivity on a reduced CO_2-basis was up to 18%, corresponding to a 4-fold improvement compared to direct electrochemical CO_2 conversion in a flow cell. Meanwhile, dilute C_3 oxygenate products could be easily isolated from the gaseous outlet stream of the second hydroformylation reactor. A similar concept was also leveraged by Li *et al.*,[126] who adopted an optimized Rh-complex catalyst for the hydroformylation reaction, increasing the C_3 oxygenate selectivity to 44%. Other carbonylation reactions such as hydrocarboxylation, alkoxycarbonylation, and aminocarbonylation are also possible, as suggested by some very recent reports.[127,128]

In addition to the major reactants, the eCO$_2$RR or eCORR can also supply activity- or selectivity-regulating species that do not directly participate in the reaction to thermochemical reactors. For instance, Sargent *et al.* showcased a different electrochemical and thermochemical route for converting CO_2 to butane (C_4H_{10}) *via* a C_1 (CO/CO_2)–C_2 (C_2H_4)–C_4 (C_4H_{10}) cascade (Fig. 8b).[129] CO in the humidified outlet stream of the direct CO_2 or CO electrolyzer was found to promote C_2H_4 dimerization to C_4H_{10} with a selectivity of up to 95% in a secondary thermochemical reactor under ambient conditions. The best overall CO-to-C_4H_{10} cascade selectivity was as high as 43%. Mechanistic insights into the role of CO were obtained through DFT calculations, demonstrating that an increase in CO coverage can result in lowered dimerization and hydrogenation barriers, both of which promote the conversion of C_2H_4 to C_4H_{10} according to the Cossee–Arlman olefin polymerization mechanism. More interestingly, a recent work by Chen *et al.* presents a proof-of-the-concept of leveraging eCO$_2$RR-derived compositionally tunable syngas (*i.e.* CO + H_2) for thermocatalytic synthesis of carbon nanofibers on the FeCo alloy under relatively mild conditions (370–450 °C, 1 atm).[130] The co-feeding of both CO and H_2 was necessary for high solid carbon yields; while with CO feed only, the FeCo alloy catalyst deactivated rapidly.

19676 | *J. Mater. Chem. A*, 2024, **12**, 19663–19684

This journal is © The Royal Society of Chemistry 2024
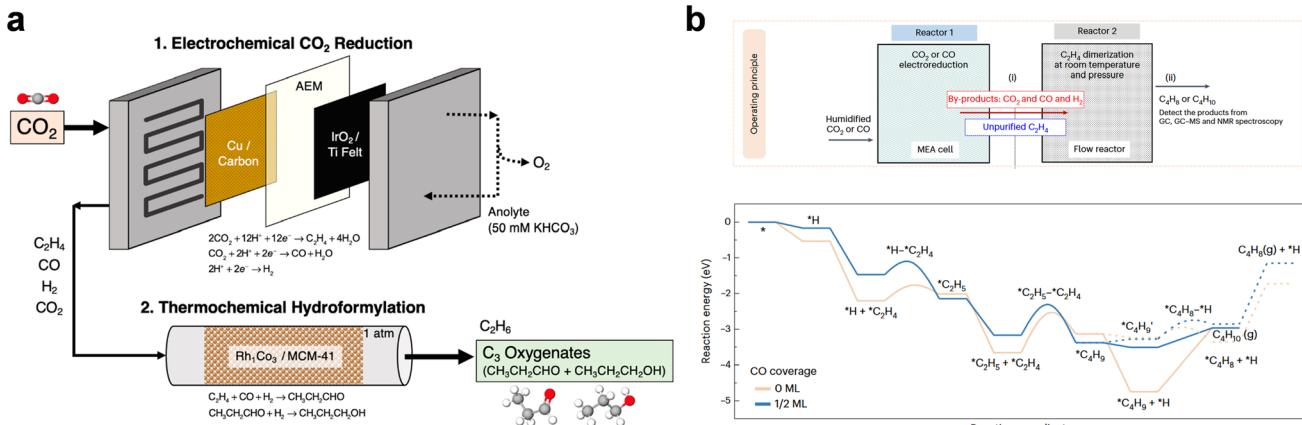
Fig. 8 "Electrochemical + thermochemical" approaches. (a) Schematic illustration of the eCO$_2$RR + hydroformylation tandem process for the synthesis of C$_3$ oxygenate products. Adapted from ref. 125 with permission from American Chemical Society. (b) (Upper) schematic illustration of the eCO$_2$RR + C$_2$H$_4$ dimerization cascade process for the synthesis of C$_4$ hydrocarbons, and (bottom) DFT-based reaction energy diagram of C$_2$H$_4$ dimerization towards C$_4$H$_{10}$ (solid lines) and C$_4$H$_8$ (short dashed lines) under 0 ML (beige) and 1/2 ML (blue) CO* coverage, respectively. Adapted from ref. 129 with permission from Springer Nature.

The above success, as well as the vast number of well-established thermochemical reactions, has demonstrated the great potential of the "electrochemical + thermochemical" approach to extend the reach of electrochemical CO$_2$ upgrading to the synthesis of C$_{3+}$ products or even advanced solid carbon materials. Other promising reactions include Fischer–Tropsch synthesis and syngas–methanol–aromatic conversion.[131,132] While the gas product stream of the eCO$_2$RR has been primarily focused on so far, the liquid product stream, such as alcohols and carboxylic acids, remains less considered for further thermochemical conversion, probably due to their low concentration in the blended electrolyte solution. A number of opportunities therefore still remain for engineering tandem or cascade "electrochemical + thermochemical" CO$_2$ conversion processes, which call for further exploration by future researchers.

3.3. "Electrochemical + biological" approaches

Similar to thermochemical reactions, there are many well-established biocatalytic reactions or processes capable of producing C$_{3+}$ chemicals with high selectivity and product specificity. More interestingly, biological processes can produce long-chain natural products that are absent in the product spectra of conventional electrolysis or thermocatalysis. For instance, glucose and fatty acids are key elements for human nutrition and important raw materials for fine chemical engineering and the food industry.[133,134] Producing them by mimicking the natural process of CO$_2$ fixation therefore presents great potential to revolutionize agriculture, reshape the bioeconomy, maintain biodiversity, and minimize the carbon footprint.[135–137] In light of this, coupling biological processes with electrocatalysis provides a potential route to this goal, where renewable electricity is adopted to transform CO$_2$ into reduced products, and various organisms or extracted enzymes are employed to produce value-added long-chain compounds from the reduced products.[138] Note that in a broader context of

bioelectrocatalysis, the electrochemical and biochemical processes can be integrated directly or indirectly. In direct bioelectrocatalysis, organisms compatible with the complex electrochemical environments are attached to catalytic electrodes directly, the number of which however remains limited. Thus, we primarily focus on the indirect coupling strategy, namely the spatially separated electro-biosystem, in this review.

Along this line, Schmid *et al.* described a scalable hybrid system by placing a fermentation module after a GDE-based CO$_2$ electrolyzer yielding syngas for subsequent anaerobic fermentation (Fig. 9a).[139] The CO$_2$ electrolyzer was carefully engineered with a commercial Ag-based GDE, exhibiting high energy efficiency of converting CO$_2$ to syngas at hundreds of mA cm^{-2}. Such a high current density is generally unattainable in the direct bioelectrolysis scheme. Two kinds of anaerobic fermenters were then adopted for the relay biochemical conversion; *C. autoethanogenum* was first responsible for converting syngas to acetate and ethanol, *C. kluyveri* was then used to convert acetate and ethanol to butyrate and hexanoate, and finally *C. autoethanogenum* was adopted again to produce 1-butanol and 1-hexanol from their corresponding carboxylates. The total carbon selectivity to C$_4$ and C$_6$ alcohols was found to be significantly higher than that of the pure electrochemical approach.

Nevertheless, the low solubility of the gas feed could limit the productivity, volumetric efficiency, and economic viability of the "electrochemical + biological" system. In this regard, liquid carbon sources remain more desirable. While formic acid and methanol have high biotoxicity, acetic acid, or acetate as its salt form, is more readily metabolizable by a broad range of organisms. Separate studies have demonstrated the feasibility of leveraging eCO$_2$RR-derived acetic acid/acetate for the biocatalytic production of long-chain organic compounds. As proposed by Xia *et al.*, acetate can be employed to organically link the two-step eCO$_2$RR-eCORR and yeast fermentation, generating glucose with high yields (Fig. 9b).[33] In the two-step

This journal is © The Royal Society of Chemistry 2024

*J. Mater. Chem. A*, 2024, **12**, 19663–19684 | **19677**
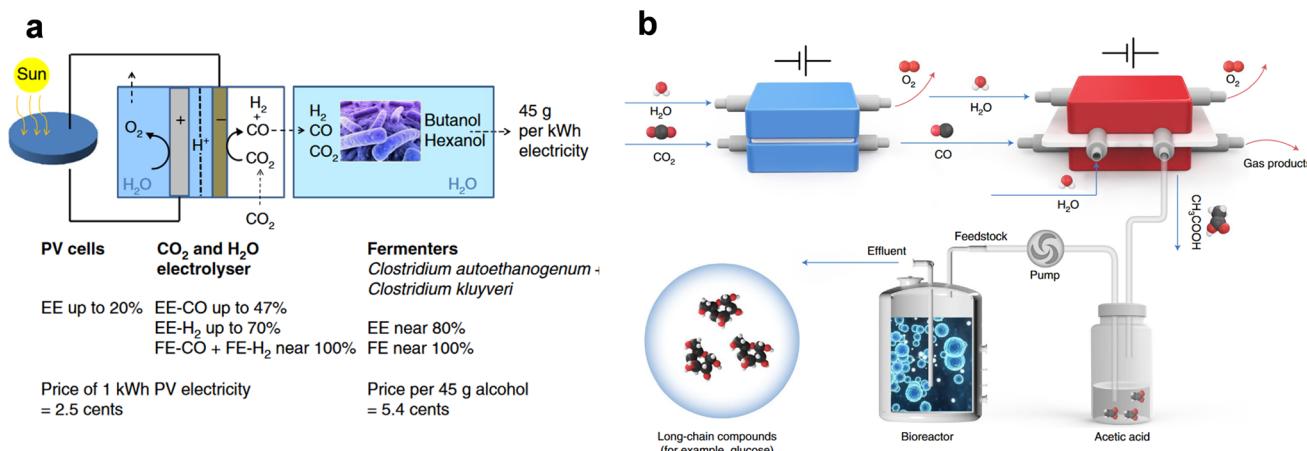
Fig. 9 "Electrochemical + biological" approaches. (a) Schematic illustration of the CO_2 electrolyzer coupled to a fermentation module for the synthesis of 1-butanol and 1-hexanol. Adapted from ref. 139 with permission from Springer Nature. (b) Schematic illustration of the *in vitro* artificial sugar synthesis system based on the two-step $eCO_2RR-eCORR$ and yeast fermentation. Adapted from ref. 33 with permission from Springer Nature.

eCO_2RR-$eCORR$ process, a Ni–N–C single atom catalyst and a defect-rich Cu catalyst were employed as the CO producer and acetate producer, achieving a FE of nearly 100% for CO from the eCO_2RR and a FE of 52% for acetate from the $eCORR$, respectively. Moreover, the adoption of a porous solid electrolyte in the second CO electrolyzer allowed for continuous generation of pure and concentrated acetic acid without pollution from electrolyte salts. The authors then genetically engineered *S. cerevisiae* to realize glucose production from the as-electrogenerated pure acetic acid *in vitro* with a high glucose yield of 8.90 μmol per gram yeast per hour. In contrast, acetate with salt impurities resulted in no glucose production. The wide applicability of this work has attracted much attention, as it can be readily extended to the production of other chemicals as well (*e.g.* free fatty acids). Nearly at the same time, Jinkerson *et al.* reported a similar two-step electrochemical CO_2-to-acetate conversion route and used acetates for the heterotrophic cultivation of food-producing organisms such as yeast, fungi, algae, and crop plants, presenting another valid example of the promising perspectives of a decoupled electro-biosystem.[34] The available products of the "electrochemical + biological" scheme have been further extended to polymers. Dai *et al.* presented a systematic multi-tier chem-bio design to seamlessly integrate the eCO_2RR with microbial metabolism.[140] By taking soluble C_2 intermediates as the feedstock, microorganisms showed better metabolic kinetics than C_1 intermediates and H_2 to produce medium-chain-length polyhydroxyalkanoates for applications such as biodegradable plastics.

In general, the technical feasibility and huge potential of "electrochemical + biological" approaches have been demonstrated by a handful of studies. The ability to produce long-chain compounds that are rarely observed in electrochemical and thermochemical CO_2 conversion by the "electrochemical + biological" approach makes it particularly attractive. In addition, biological processes usually require only mild reaction conditions, in contrast to the majority of thermochemical

processes demanding elevated temperature or pressure, which can be valuable for process decentralization.

4. Summary and outlook

Due to the higher energy density and economic value of C_{3+} fuels and chemicals than their C_1 and C_2 counterparts, upgrading CO_2 to C_{3+} products with renewable electricity is undoubtedly a promising direction to realize "Net Zero" emission and lay the foundation for a sustainable chemical industry. In the past few decades, many efforts have been devoted to the development and optimization of direct eCO_2RR technologies, showing a great leap in C_3 selectivity and activity. Aiming to produce C_{4+} species with higher molecular weights, coupling the eCO_2RR with a complementary process has emerged in recent years to allow for tandem or cascade conversion leveraging reduced products in the outlet stream of the eCO_2RR. Despite the continuous research progress and constantly renewed records of C_{3+} selectivity/activity, challenges towards industrialization persist. Here we discuss some perspectives on these challenges and opportunities for addressing them.

4.1. Direct electrochemical approach

The direct electrochemical approach presents the simplest way of converting CO_2 to C_{3+} products as the least number of processes are involved. The overall process can often run at near room temperature and ambient pressure. Along with the scalability of electrolyzers, this approach is extremely suitable for decentralized applications. To reveal the general trend of the eCO_2RR/$eCORR$ to C_{3+} products, the optimal FE and partial current density ($j_{C_{3+}}$) of C_{3+} products are summarized in Table S1† and Fig. 10. It can be generally concluded that after decades of research, the conversion efficiency of CO_2 to a specific C_{3+} product is still the major bottleneck of direct CO_2 electrolysis.

In addition to the above general conclusion, several key aspects can be extracted from Fig. 10: (1) the structural

19678 | *J. Mater. Chem. A*, 2024, **12**, 19663–19684

This journal is © The Royal Society of Chemistry 2024
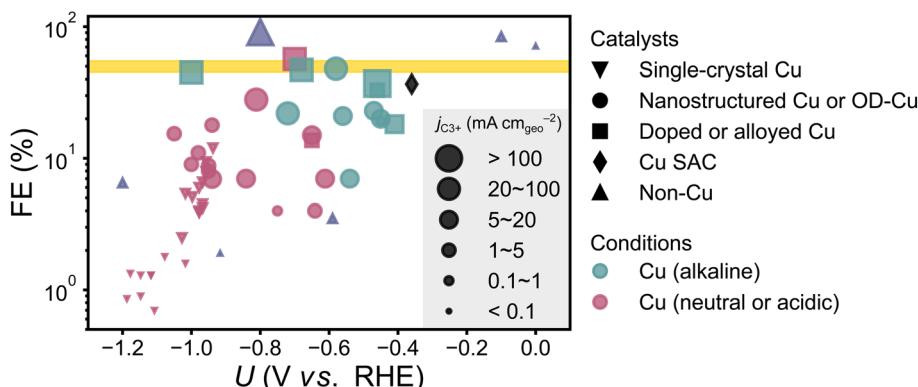
Fig. 10   A summary on catalytic performance of direct electrochemical CO_2/CO-to-C_{3+} conversion using different types of catalysts (including single-crystal Cu, nanostructured Cu or OD-Cu, doped or alloyed Cu with foreign element regulation, Cu SAC, and Mo- or Ni-based non-Cu catalysts). The first three types of catalysts are further divided into two groups to reveal the influence of electrolyte pH; cyan for the alkaline conditions where KOH electrolytes are adopted, and red for the neutral or acidic conditions where bicarbonates, halides, or other oxysalts are adopted. The size of markers indicates the magnitude of partial current density of C_{3+} formation. Data for plotting are tabulated in Table S1.†

sensitivity of Cu-based catalysts. With Cu-based materials still being the only widely justified catalytic systems for the eCO$_2$RR to C_{3+} chemicals, most of the reports have demonstrated optimal FEs of 5–15%, which is quite close to the results obtained on single-crystal Cu(S)-[n(100) × (111)] electrodes according to the 20 year-old report by Hori *et al.*[56] This finding accentuates the necessity of combining different Cu sites with distinct coordination numbers, local geometries and electronic structures, and binding affinities to critical surface species (*e.g.* CO and C_2 precursors). Therefore, a focus shift from active site to active site ensemble may facilitate future Cu-based catalyst design. By comparing the nanostructure Cu/OD-Cu (shown as circles in Fig. 10) systems with doped/alloyed Cu (shown as squares in Fig. 10) systems, it is found that dilute alloying presents the most promising route for selective C_3 production; nevertheless, we also note that these bimetallic or multimetallic materials still benefit from desirable micro-/nanostructure and defect-rich surfaces. Untangling the intertwined structural and electronic effects is still of great interest from a fundamental perspective.

(2) The conditional sensitivity of direct electrolysis. CO_2/CO electrolysis under alkaline conditions (shown in cyan in Fig. 10) generally demonstrates higher catalytic efficiency than electrolysis under neutral or acidic conditions (shown in red in Fig. 10). This is in accordance with the well-understood pH effect that high pH favors C_2 formation, giving rise to higher coverage of C_2 for further coupling reactions.[36–42] Also, the HER is suppressed at high alkalinity. However, it must be pointed out that the inevitable reaction between CO_2 and hydroxide is detrimental to the local alkalinity maintenance and overall carbon efficiency. The conversion from CO_2 to CO is suggested to be spatially decoupled from the subsequent CO-to-C_{3+} process; otherwise, improving the catalytic efficiency in acidic media would be another promising direction.

(3) The narrow optimal operational window. Through combinatorial efforts in engineering catalysts, CO_2/CO feedings, reaction microenvironments, and reactors, the highest C_3

FEs were reported in the range of approximately 45–55% (highlighted as the region in yellow, Fig. 10). However, such an optimal performance is only attainable in a quite narrow potential (or current-density) window,[104,106] severely limiting the compatibility of pure electrochemical systems with renewable power generations showing huge variations in output current. Therefore, it is necessary to further widen the high-C_3-selectivity window for practical decentralized applications.

(4) The inherent mechanistic limitations of the carbonyl-dominated C–C coupling mechanism. It is rare for Cu-based catalytic systems to yield products beyond C_3 through direct eCO$_2$RR. Although recent studies have validated the possibility to produce C_{4+} through domino reactions coupling homogeneous non-electrocatalytic and heterogeneous electrocatalytic steps in one-pot electrolysis, their FEs are at the level of ~20%, far from satisfactory for industrialization.[121,122] The lack or scarcity of C_{4+} products in the Cu-catalyzed eCO$_2$RR suggests the inherent limitation of the carbonyl-dominated C–C coupling mechanism. On one hand, moderately binding catalytic surfaces like Cu are essential for suppressing the HER. On the other hand, high CO* coverage is essential for the initial C–C bond formation. Nonetheless, it is difficult to obtain sufficient coverage of higher-order C_{2+} as well under such a prerequisite. Balancing the surface distribution of various key C_1–C_3 intermediates would require a variety of active site ensembles possessing different propensities to bind specific intermediates. This could explain the high structural sensitivity of Cu-based catalysts. However, Cu surfaces are often extremely sensitive to the environment and quite dynamic under specific reaction conditions,[66–68] which is in stark contradiction to the above requirements to stabilize C_3-specific active site ensembles and balance the propensities of key surface intermediates. The origin of the above limitation still remains a missing piece in the current mechanistic understanding of the eCO$_2$RR. Further investigations combining advanced characterization and simulation tools to reveal corresponding mechanistic understandings therefore remain nontrivial.

(5) The promise and problem of non-Cu catalysts. Exploring non-Cu catalysts having different mechanisms (*e.g.* hydrocarbon oligomerization and oxygenate condensation) can effectively circumvent the above fundamental limitations that conventional Cu-based catalysts may pose. As a consequence, some non-Cu catalysts such as Mo and Ni phosphides have shown very promising FEs (>90%) and overpotentials (<300 mV) for C_3 production (Fig. 10).[116,119] These Mo- and Ni-based non-Cu catalysts generally feature intermediate chemisorption strengths between Cu and strong-binding surfaces known for being HER-active only (*e.g.* Ni metal), allowing for favorable stabilization of certain C_{2+} surface species. However, the enhancement of the HER can emerge as an undesirable side effect.[118] Therefore, the increased carbon selectivity towards C_{3+} usually comes at the price of lowered electron selectivity, which is also the main reason why C_3 FE decreases drastically with increasing overpotential (Fig. 10). Seeking appropriate HER-suppression strategies without sacrificing the unique C_{3+} productivity is a promising future direction. As the exploration of novel non-Cu catalysts is less reported than that of Cu-based catalysts, more justification on the validity of non-Cu catalysts for both carbon- and electron-selective eCO$_2$RR would be necessary.

4.2. "Electrochemical + X" approaches

Compared to pure electrochemical approaches, "electrochemical + X" approaches present several unique advantages (Table 1). The first exceptional advantage lies in the high production efficiency (combining both selectivity and activity) of C_{3+} products from CO_2. This is attributed to the discrete nature of process units, which allows for individual design and separate optimization of each unit without interference from other processes, as opposed to reactions in one pot. Moreover, complementing a spatially decoupled "X" process can strictly isolate the needs for CO_2 activation and C–C coupling into different sectors. And the vast possibilities in complementary

processes significantly expand the product scope from single-electrolysis-accessible C_3/C_4 alcohols and hydrocarbons to inaccessible C_{5+} chemicals. In addition, we propose that the spatially separated yet still in-place tandem process is more advantageous than deploying multiple individual plants in different locations, due to the elimination of safety risks associated with long-range transportation and long-term storage of hazardous chemicals (*e.g.* CO and H_2).

However, "electrochemical + X" approaches also face a series of challenges for practical implementation: (1) the system complexity is higher than that of the direct electrochemical approaches as there are more unit processes, which inevitably results in increased costs for construction, operation, and maintenance, offsetting the benefits of more valuable C_{4+} chemicals as well as their enhanced yields in a tandem process. More importantly, some of the "X" processes, especially thermochemical reactions demanding high temperature and pressure, are obviously energy-intense and carbon-emission-positive, while biological processes often rely on non-autotrophic organisms, the life maintenance of which also needs extra energy inputs and emits CO_2. Both aspects mitigate the ability of such hybrid approaches to reduce CO_2 emission compared to their purely renewable-powered electrochemical counterparts. Therefore, critical techno-economic and carbon footprint analyses are of utmost urgency and importance in future research, especially for unexplored products (*e.g.* aromatics).

(2) Another key aspect is the interaction between electrochemical and complementary modules. The product outlet streams of the eCO$_2$RR are typically mixed gas and liquid products, as currently it is only possible to control the product selectivity to near-unity for $2e^-$ products (CO and formate) *via* the eCO$_2$RR. Although some studies have showcased the possibility of leveraging a mixture feedstock without purification,[125,129] the influence of impurities is usually nontrivial and deserves in-depth investigations.[33,34] Implementation of extra separation units can further introduce economic burden. In

Table 1 A summary on advantages and challenges of "electrochemical + X" and direct electrochemical approaches for upgrading CO_2 to C_{3+} products

	"Electrochemical + X"	Direct electrochemical
Advantages	• High conversion efficiency • Decoupled process optimization • Expanded scope of available products • Eliminate risky chemical transportation and storage	• Simple processes • Mild conditions • Suitable for decentralized applications
Challenges	*Overall* • Complex processes • Increased capitalized costs • Interface or connection between modules (*e.g.* stream purification) "X" – *homogeneous reactions* • Reaction rate alignment • Mass-transport management of reactive intermediates "X" – *thermochemical* • Additional energy consumption and CO_2 emission • Unsuitable for decentralized applications "X" – *biological* • Extra energy input for non-autotrophic organisms, and CO_2 emission • Product separation from organisms	*Cu-based catalytic systems* • Low conversion efficiency • Limited availability of products • Narrow operational window *Non-Cu catalytic systems* • HER competition • Wider and more rigorous demonstration

19680 | *J. Mater. Chem. A*, 2024, **12**, 19663–19684

This journal is © The Royal Society of Chemistry 2024

this case, adoption of solid-electrolyte-based electrolyzers may alleviate the issue of separating liquid products from electrolyte salts.[33] Seeking complementary approaches with high tolerance to impurities or capabilities to utilize multiple feedstocks presents another promising future direction. Apart from the inlet stream purification, the separation of products and organisms also presents a technical hurdle and deserves further techno-economic analyses and investigations.

(3) The actual efficiencies of "electrochemical + X" approaches require more rigorous and comprehensive evaluation. There are a number of factors leading to deteriorated efficiency. For "electrochemical + homogeneous reaction" approaches, homogeneous reactions (e.g. aldol condensation or esterification) under ambient conditions often possess lower rates than the prior electrochemical reactions, limiting the conversion of C_{1-3} intermediates to C_{4+} products.[121,122] The mass transport of reactive intermediates also needs to be well managed towards full utilization. When "X" stands for thermochemical or biological processes, the overall energy efficiency might not be as promising as the conversion efficiency (based on either carbon or electron utilization). The extra energy required for driving thermochemical reactions or sustaining organism lifespan is nontrivial, and developing better practices to maintain the superiority of "electrochemical + X" remains indispensable.

In sum, the electrochemical upgrading of CO_2 to high-value C_{3+} products has remained and will stay a challenging yet attractive research area for decades to come. Collaborative research studies from multidisciplinary and interdisciplinary perspectives are highly desirable to spur innovations on advanced materials and processes. And we believe that the successful industrialization of electrochemical and sustainable CO_2 upgrading will eventually present a viable solution to the environmental and energy crises faced by human society.

Data availability

No primary research results have been included and no new data were generated or analyzed as part of this review.

Conflicts of interest

The authors have no competing interests.

Acknowledgements

References

1 J. D. Shakun, P. U. Clark, F. He, S. A. Marcott, A. C. Mix, Z. Liu, B. Otto-Bliesner, A. Schmittner and E. Bard, Nature, 2012, 484, 49–54.

2 P. M. Cox, R. A. Betts, C. D. Jones, S. A. Spall and I. J. Totterdell, Nature, 2000, 408, 184–187.

3 O. S. Bushuyev, P. De Luna, C. T. Dinh, L. Tao, G. Saur, J. van de lagemaat, S. O. Kelley and E. H. Sargent, Joule, 2018, 2, 825–832.

4 E. S. Sanz-Pérez, C. R. Murdock, S. A. Didas and C. W. Jones, Chem. Rev., 2016, 116, 11840–11876.

5 S. Mehla, A. E. Kandjani, R. Babarao, A. F. Lee, S. Periasamy, K. Wilson, S. Ramakrishna and S. K. Bhargava, Energy Environ. Sci., 2021, 14, 320–352.

6 K. U. D. Calvinho, A. B. Laursen, K. M. K. Yap, T. A. Goetjen, S. Hwang, N. Murali, B. Mejia-Sosa, A. Lubarski, K. M. Teeluck, E. S. Hall, E. Garfunkel, M. Greenblatt and G. C. Dismukes, Energy Environ. Sci., 2018, 11, 2550–2559.

7 K. Schuchmann and V. Müller, Nat. Rev. Microbiol., 2014, 12, 809–821.

8 Y. Song, J. S. Lee, J. Shin, G. M. Lee, S. Jin, S. Kang, J.-K. Lee, D. R. Kim, E. Y. Lee, S. C. Kim, S. Cho, D. Kim and B.-K. Cho, Proc. Natl. Acad. Sci. U. S. A., 2020, 117, 7516–7523.

9 G. Yang, P. Qiu, J. Xiong, X. Zhu and G. Cheng, Chin. Chem. Lett., 2022, 33, 3709–3712.

10 S. Bai, H. Qiu, M. Song, G. He, F. Wang, Y. Liu and L. Guo, eScience, 2022, 2, 428–437.

11 S. Ng, J. J. Foo and W. Ong, InfoMat, 2022, 4, e12279.

12 T. Jia, L. Wang, Z. Zhu, B. Zhu, Y. Zhou, G. Zhu, M. Zhu and H. Tao, Chin. Chem. Lett., 2024, 35, 108692.

13 Q. Zhu, J. Ma, X. Kang, X. Sun, J. Hu, G. Yang and B. Han, Sci. China: Chem., 2016, 59, 551–556.

14 Y. Luo, K. Zhang, Y. Li and Y. Wang, InfoMat, 2021, 3, 1313–1332.

15 D. Song, Y. Lian, M. Wang, Y. Su, F. Lyu, Z. Deng and Y. Peng, eScience, 2023, 3, 100097.

16 J. Qiao, Y. Liu, F. Hong and J. Zhang, Chem. Soc. Rev., 2014, 43, 631–675.

17 J. Gu, C.-S. Hsu, L. Bai, H. M. Chen and X. Hu, Science, 2019, 364, 1091–1094.

18 R. Shi, J. Guo, X. Zhang, G. I. N. Waterhouse, Z. Han, Y. Zhao, L. Shang, C. Zhou, L. Jiang and T. Zhang, Nat. Commun., 2020, 11, 3028.

19 K. Xu, S. Zheng, Y. Li, H. Chu, Q. Xiong, Z. Mei, Q. Zhao, L. Yang, S. Li and F. Pan, Chin. Chem. Lett., 2022, 33, 424–427.

20 Y. Wu, Z. Jiang, X. Lu, Y. Liang and H. Wang, Nature, 2019, 575, 639–642.

21 L. Lu, X. Sun, J. Ma, D. Yang, H. Wu, B. Zhang, J. Zhang and B. Han, Angew. Chem., Int. Ed., 2018, 57, 14149–14153.

22 B. Yang, L. Li, Z. Jia, X. Liu, C. Zhang and L. Guo, Chin. Chem. Lett., 2020, 31, 2627–2633.

23 J. Du, S. Li, S. Liu, Y. Xin, B. Chen, H. Liu and B. Han, Chem. Sci., 2020, 11, 5098–5104.

24 Y. Yang, J. Fu, Y. Ouyang, T. Tang, Y. Zhang, L.-R. Zheng, Q.-H. Zhang, X.-Z. Liu, J. Wang and J.-S. Hu, Natl. Sci. Rev., 2023, 10, nwac248.

25 H. H. Wong, M. Sun, T. Wu, C. H. Chan, L. Lu, Q. Lu, B. Chen and B. Huang, eScience, 2024, 4, 100140.

This journal is © The Royal Society of Chemistry 2024

J. Mater. Chem. A, 2024, 12, 19663–19684 | 19681

26 T. T. H. Hoang, S. Verma, S. Ma, T. T. Fister, J. Timoshenko, A. I. Frenkel, P. J. A. Kenis and A. A. Gewirth, *J. Am. Chem. Soc.*, 2018, **140**, 5791–5797.

27 Z. Chen, T. Wang, B. Liu, D. Cheng, C. Hu, G. Zhang, W. Zhu, H. Wang, Z.-J. Zhao and J. Gong, *J. Am. Chem. Soc.*, 2020, **142**, 6878–6883.

28 T. Qin, Y. Qian, F. Zhang and B.-L. Lin, *Chin. Chem. Lett.*, 2019, **30**, 314–318.

29 L. Tao, E. C. D. Tan, R. McCormick, M. Zhang, A. Aden, X. He and B. T. Zigler, *Biofuels, Bioprod. Biorefin.*, 2014, **8**, 30–48.

30 K. P. Kuhl, E. R. Cave, D. N. Abram and T. F. Jaramillo, *Energy Environ. Sci.*, 2012, **5**, 7050–7059.

31 P. Dürre, *Biotechnol. J.*, 2007, **2**, 1525–1534.

32 G. R. M. Dowson, M. F. Haddow, J. Lee, R. L. Wingad and D. F. Wass, *Angew. Chem., Int. Ed.*, 2013, **52**, 9005–9008.

33 T. Zheng, M. Zhang, L. Wu, S. Guo, X. Liu, J. Zhao, W. Xue, J. Li, C. Liu, X. Li, Q. Jiang, J. Bao, J. Zeng, T. Yu and C. Xia, *Nat. Catal.*, 2022, **5**, 388–396.

34 E. C. Hann, S. Overa, M. Harland-Dunaway, A. F. Narvaez, D. N. Le, M. L. Orozco-Cárdenas, F. Jiao and R. E. Jinkerson, *Nat. Food*, 2022, **3**, 461–471.

35 N. S. Romero Cuellar, K. Wiesner-Fleischer, M. Fleischer, A. Rucki and O. Hinrichsen, *Electrochim. Acta*, 2019, **307**, 164–175.

36 K. G. Schulz, U. Riebesell, B. Rost, S. Thoms and R. E. Zeebe, *Mar. Chem.*, 2006, **100**, 53–65.

37 K. J. P. Schouten, E. Pérez Gallent and M. T. M. Koper, *J. Electroanal. Chem.*, 2014, **716**, 53–57.

38 A. S. Varela, M. Kroschel, T. Reier and P. Strasser, *Catal. Today*, 2016, **260**, 8–13.

39 X. Liu, P. Schlexer, J. Xiao, Y. Ji, L. Wang, R. B. Sandberg, M. Tang, K. S. Brown, H. Peng, S. Ringe, C. Hahn, T. F. Jaramillo, J. K. Nørskov and K. Chan, *Nat. Commun.*, 2019, **10**, 32.

40 J. C. Bui, C. Kim, A. Z. Weber and A. T. Bell, *ACS Energy Lett.*, 2021, **6**, 1181–1188.

41 C. Kim, J. C. Bui, X. Luo, J. K. Cooper, A. Kusoglu, A. Z. Weber and A. T. Bell, *Nat. Energy*, 2021, **6**, 1026–1034.

42 H.-J. Peng, M. T. Tang, J. Halldin Stenlid, X. Liu and F. Abild-Pedersen, *Nat. Commun.*, 2022, **13**, 1399.

43 J. Lee, Y. Kwon, R. L. Machunda and H. J. Lee, *Chem.–Asian J.*, 2009, **4**, 1516–1523.

44 Y. Hori, A. Murata, R. Takahashi and S. Suzuki, *J. Chem. Soc. Chem. Commun.*, 1988, 17.

45 J. H. Montoya, C. Shi, K. Chan and J. K. Nørskov, *J. Phys. Chem. Lett.*, 2015, **6**, 2032–2037.

46 R. Kortlever, J. Shen, K. J. P. Schouten, F. Calle-Vallejo and M. T. M. Koper, *J. Phys. Chem. Lett.*, 2015, **6**, 4073–4082.

47 T. Cheng, H. Xiao and W. A. Goddard, *Proc. Natl. Acad. Sci. U. S. A.*, 2017, **114**, 1795–1800.

48 D. Ren, N. T. Wong, A. D. Handoko, Y. Huang and B. S. Yeo, *J. Phys. Chem. Lett.*, 2016, **7**, 20–24.

49 Y. Hori, R. Takahashi, Y. Yoshinami and A. Murata, *J. Phys. Chem. B*, 1997, **101**, 7075–7081.

50 X. Liu, J. Xiao, H. Peng, X. Hong, K. Chan and J. K. Nørskov, *Nat. Commun.*, 2017, **8**, 15438.

51 Y. Pang, J. Li, Z. Wang, C.-S. Tan, P.-L. Hsieh, T.-T. Zhuang, Z.-Q. Liang, C. Zou, X. Wang, P. De Luna, J. P. Edwards, Y. Xu, F. Li, C.-T. Dinh, M. Zhong, Y. Lou, D. Wu, L.-J. Chen, E. H. Sargent and D. Sinton, *Nat. Catal.*, 2019, **2**, 251–258.

52 H. Xiao, T. Cheng and W. A. I. Goddard, *J. Am. Chem. Soc.*, 2017, **139**, 130–136.

53 L. Chen, C. Tang, Y. Zheng, E. Skúlason and Y. Jiao, *J. Mater. Chem. A*, 2022, **10**, 5998–6006.

54 M. T. Tang, H.-J. Peng, J. H. Stenlid and F. Abild-Pedersen, *J. Phys. Chem. C*, 2021, **125**, 26437–26447.

55 S. Pablo-García, F. L. P. Veenstra, L. R. L. Ting, R. García-Muelas, F. Dattila, A. J. Martín, B. S. Yeo, J. Pérez-Ramírez and N. López, *Catal. Sci. Technol.*, 2022, **12**, 409–417.

56 Y. Hori, I. Takahashi, O. Koga and N. Hoshi, *J. Mol. Catal. A: Chem.*, 2003, **199**, 39–47.

57 Y.-T. Chan, I.-S. Huang and M.-K. Tsai, *Phys. Chem. Chem. Phys.*, 2019, **21**, 22704–22710.

58 C.-C. Chang, M.-S. Ku, W.-H. Lien and S.-F. Hung, *J. Phys. Chem. C*, 2022, **126**, 5502–5512.

59 X. Chang, A. Malkani, X. Yang and B. Xu, *J. Am. Chem. Soc.*, 2020, **142**, 2975–2983.

60 Y. Hori, I. Takahashi, O. Koga and N. Hoshi, *J. Phys. Chem. B*, 2002, **106**, 15–17.

61 M. A. Van Hove and G. A. Somorjai, *Surf. Sci.*, 1980, **92**, 489–518.

62 M. Wu, Z. Zhang, X. Xu, Z. Zhang, Y. Duan, J. Dong, R. Qiao, S. You, L. Wang, J. Qi, D. Zou, N. Shang, Y. Yang, H. Li, L. Zhu, J. Sun, H. Yu, P. Gao, X. Bai, Y. Jiang, Z.-J. Wang, F. Ding, D. Yu, E. Wang and K. Liu, *Nature*, 2020, **581**, 406–410.

63 S. Jin, M. Huang, Y. Kwon, L. Zhang, B.-W. Li, S. Oh, J. Dong, D. Luo, M. Biswal, B. V. Cunning, P. V. Bakharev, I. Moon, W. J. Yoo, D. C. Camacho-Mojica, Y.-J. Kim, S. H. Lee, B. Wang, W. K. Seong, M. Saxena, F. Ding, H.-J. Shin and R. S. Ruoff, *Science*, 2018, **362**, 1021–1025.

64 C. Zhu, Z. Zhang, L. Zhong, C.-S. Hsu, X. Xu, Y. Li, S. Zhao, S. Chen, J. Yu, S. Chen, M. Wu, P. Gao, S. Li, H. M. Chen, K. Liu and L. Zhang, *Chem*, 2021, **7**, 406–420.

65 R. Reske, H. Mistry, F. Behafarid, B. Roldan Cuenya and P. Strasser, *J. Am. Chem. Soc.*, 2014, **136**, 6978–6986.

66 D. Kim, C. S. Kley, Y. Li and P. Yang, *Proc. Natl. Acad. Sci. U. S. A.*, 2017, **114**, 10560–10565.

67 Y. Li, D. Kim, S. Louisia, C. Xie, Q. Kong, S. Yu, T. Lin, S. Aloni, S. C. Fakra and P. Yang, *Proc. Natl. Acad. Sci. U. S. A.*, 2020, **117**, 9194–9201.

68 J. Liu, F. You, B. He, Y. Wu, D. Wang, W. Zhou, C. Qian, G. Yang, G. Liu, H. Wang, Y. Guo, L. Gu, L. Feng, S. Li and Y. Zhao, *J. Am. Chem. Soc.*, 2022, **144**, 12410–12420.

69 W.-Y. Zhi, Y.-T. Liu, S.-L. Shan, C.-J. Jiang, H. Wang and J.-X. Lu, *J. CO2 Util.*, 2021, **50**, 101594.

70 C. Liu, M. Zhang, J. Li, W. Xue, T. Zheng, C. Xia and J. Zeng, *Angew. Chem., Int. Ed.*, 2022, **61**, e202113498.

71 P.-P. Yang, X.-L. Zhang, F.-Y. Gao, Y.-R. Zheng, Z.-Z. Niu, X. Yu, R. Liu, Z.-Z. Wu, S. Qin, L.-P. Chi, Y. Duan, T. Ma, X.-S. Zheng, J.-F. Zhu, H.-J. Wang, M.-R. Gao and S.-H. Yu, *J. Am. Chem. Soc.*, 2020, **142**, 6400–6408.

19682 | *J. Mater. Chem. A*, 2024, **12**, 19663–19684

This journal is © The Royal Society of Chemistry 2024

72 K. D. Yang, W. R. Ko, J. H. Lee, S. J. Kim, H. Lee, M. H. Lee and K. T. Nam, *Angew. Chem., Int. Ed.*, 2017, **56**, 796–800.

73 T.-T. Zhuang, Y. Pang, Z.-Q. Liang, Z. Wang, Y. Li, C.-S. Tan, J. Li, C. T. Dinh, P. De Luna, P.-L. Hsieh, T. Burdyny, H.-H. Li, M. Liu, Y. Wang, F. Li, A. Proppe, A. Johnston, D.-H. Nam, Z.-Y. Wu, Y.-R. Zheng, A. H. Ip, H. Tan, L.-J. Chen, S.-H. Yu, S. O. Kelley, D. Sinton and E. H. Sargent, *Nat. Catal.*, 2018, **1**, 946–951.

74 H. Du, L.-X. Liu, P. Li, Q. Min, S. Guo and W. Zhu, *ACS Nano*, 2023, **17**, 8663–8670.

75 C. Peng, G. Luo, J. Zhang, M. Chen, Z. Wang, T.-K. Sham, L. Zhang, Y. Li and G. Zheng, *Nat. Commun.*, 2021, **12**, 1580.

76 P. De Luna, R. Quintero-Bermudez, C.-T. Dinh, M. B. Ross, O. S. Bushuyev, P. Todorović, T. Regier, S. O. Kelley, P. Yang and E. H. Sargent, *Nat. Catal.*, 2018, **1**, 103–110.

77 D. Zhong, Z.-J. Zhao, Q. Zhao, D. Cheng, B. Liu, G. Zhang, W. Deng, H. Dong, L. Zhang, J. Li, J. Li and J. Gong, *Angew. Chem., Int. Ed.*, 2021, **60**, 4879–4885.

78 C. Long, K. Wan, Y. Chen, L. Li, Y. Jiang, C. Yang, Q. Wu, G. Wu, P. Xu, J. Li, X. Shi, Z. Tang and C. Cui, *J. Am. Chem. Soc.*, 2024, **146**, 4632–4641.

79 T.-T. Zhuang, Z.-Q. Liang, A. Seifitokaldani, Y. Li, P. De Luna, T. Burdyny, F. Che, F. Meng, Y. Min, R. Quintero-Bermudez, C. T. Dinh, Y. Pang, M. Zhong, B. Zhang, J. Li, P.-N. Chen, X.-L. Zheng, H. Liang, W.-N. Ge, B.-J. Ye, D. Sinton, S.-H. Yu and E. H. Sargent, *Nat. Catal.*, 2018, **1**, 421–428.

80 A. Loiudice, P. Lobaccaro, E. A. Kamali, T. Thao, B. H. Huang, J. W. Ager and R. Buonsanti, *Angew. Chem., Int. Ed.*, 2016, **55**, 5789–5792.

81 T. Cheng, H. Xiao and W. A. Goddard, *J. Am. Chem. Soc.*, 2017, **139**, 11642–11645.

82 C. W. Li, J. Ciston and M. W. Kanan, *Nature*, 2014, **508**, 504–507.

83 C. Long, X. Liu, K. Wan, Y. Jiang, P. An, C. Yang, G. Wu, W. Wang, J. Guo, L. Li, K. Pang, Q. Li, C. Cui, S. Liu, T. Tan and Z. Tang, *Sci. Adv.*, 2023, **9**, eadi6119.

84 A. Eilert, F. Cavalca, F. S. Roberts, J. Osterwalder, C. Liu, M. Favaro, E. J. Crumlin, H. Ogasawara, D. Friebel, L. G. M. Pettersson and A. Nilsson, *J. Phys. Chem. Lett.*, 2017, **8**, 285–290.

85 R. M. Arán-Ais, F. Scholten, S. Kunze, R. Rizo and B. Roldan Cuenya, *Nat. Energy*, 2020, **5**, 317–325.

86 J. Timoshenko, A. Bergmann, C. Rettenmaier, A. Herzog, R. M. Arán-Ais, H. S. Jeon, F. T. Haase, U. Hejral, P. Grosse, S. Kühl, E. M. Davis, J. Tian, O. Magnussen and B. Roldan Cuenya, *Nat. Catal.*, 2022, **5**, 259–267.

87 H. Xiao, W. A. Goddard, T. Cheng and Y. Liu, *Proc. Natl. Acad. Sci. U. S. A.*, 2017, **114**, 6685–6688.

88 F. Dattila, R. García-Muelas and N. López, *ACS Energy Lett.*, 2020, **5**, 3176–3184.

89 H.-Y. Wang, M. Soldemo, D. Degerman, P. Lömker, C. Schlueter, A. Nilsson and P. Amann, *Angew. Chem., Int. Ed.*, 2022, **61**, e202111021.

90 S. Lee, D. Kim and J. Lee, *Angew. Chem., Int. Ed.*, 2015, **54**, 14701–14705.

91 D. Kim, S. Lee, J. D. Ocon, B. Jeong, J. K. Lee and J. Lee, *Phys. Chem. Chem. Phys.*, 2015, **17**, 824–830.

92 Z. Lian, F. Dattila and N. López, *Nat. Catal.*, 2024, **7**, 401–411.

93 T. He, G. Kour, X. Mao and A. Du, *J. Catal.*, 2020, **382**, 49–56.

94 D. Liu, Y. Hu, E. Shoko, H. Yu, T. T. Isimjan and X. Yang, *Electrochim. Acta*, 2021, **365**, 137343.

95 Y. Hori, H. Wakebe, T. Tsukamoto and O. Koga, *Electrochim. Acta*, 1994, **39**, 1833–1839.

96 D. Ren, B. S.-H. Ang and B. S. Yeo, *ACS Catal.*, 2016, **6**, 8239–8247.

97 S. Ma, M. Sadakiyo, M. Heima, R. Luo, R. T. Haasch, J. I. Gold, M. Yamauchi and P. J. A. Kenis, *J. Am. Chem. Soc.*, 2017, **139**, 47–50.

98 E. L. Clark, C. Hahn, T. F. Jaramillo and A. T. Bell, *J. Am. Chem. Soc.*, 2017, **139**, 15848–15857.

99 L. Wang, D. C. Higgins, Y. Ji, C. G. Morales-Guio, K. Chan, C. Hahn and T. F. Jaramillo, *Proc. Natl. Acad. Sci. U. S. A.*, 2020, **117**, 12572–12575.

100 J. Li, H. Xiong, X. Liu, D. Wu, D. Su, B. Xu and Q. Lu, *Nat. Commun.*, 2023, **14**, 698.

101 M. Rahaman, K. Kiran, I. Z. Montiel, V. Grozovski, A. Dutta and P. Broekmann, *Green Chem.*, 2020, **22**, 6497–6509.

102 S. Jeong, C. Huang, Z. Levell, R. X. Skalla, W. Hong, N. J. Escorcia, Y. Losovyj, B. Zhu, A. N. Butrum-Griffith, Y. Liu, C. W. Li, D. Reifsnyder Hickey, Y. Liu and X. Ye, *J. Am. Chem. Soc.*, 2024, **146**, 4508–4520.

103 X. Wang, P. Ou, A. Ozden, S.-F. Hung, J. Tam, C. M. Gabardo, J. Y. Howe, J. Sisler, K. Bertens, F. P. García de Arquer, R. K. Miao, C. P. O'Brien, Z. Wang, J. Abed, A. S. Rasouli, M. Sun, A. H. Ip, D. Sinton and E. H. Sargent, *Nat. Energy*, 2022, **7**, 170–176.

104 K. Qi, Y. Zhang, N. Onofrio, E. Petit, X. Cui, J. Ma, J. Fan, H. Wu, W. Wang, J. Li, J. Liu, Y. Zhang, Y. Wang, G. Jia, J. Wu, L. Lajaunie, C. Salameh and D. Voiry, *Nat. Catal.*, 2023, **6**, 319–331.

105 X. Wang, Z. Wang, T.-T. Zhuang, C.-T. Dinh, J. Li, D.-H. Nam, F. Li, C.-W. Huang, C.-S. Tan, Z. Chen, M. Chi, C. M. Gabardo, A. Seifitokaldani, P. Todorović, A. Proppe, Y. Pang, A. R. Kirmani, Y. Wang, A. H. Ip, L. J. Richter, B. Scheffel, A. Xu, S.-C. Lo, S. O. Kelley, D. Sinton and E. H. Sargent, *Nat. Commun.*, 2019, **10**, 5186.

106 H. Phong Duong, J. G. Rivera de la Cruz, N.-H. Tran, J. Louis, S. Zanna, D. Portehault, A. Zitolo, M. Walls, D. V. Peron, M. W. Schreiber, N. Menguy and M. Fontecave, *Angew. Chem., Int. Ed.*, 2023, **62**, e202310788.

107 A. H. M. da Silva, Q. Lenne, R. E. Vos and M. T. M. Koper, *ACS Catal.*, 2023, **13**, 4339–4347.

108 W. Niu, Z. Chen, W. Guo, W. Mao, Y. Liu, Y. Guo, J. Chen, R. Huang, L. Kang, Y. Ma, Q. Yan, J. Ye, C. Cui, L. Zhang, P. Wang, X. Xu and B. Zhang, *Nat. Commun.*, 2023, **14**, 4882.

109 K. Zhao, X. Nie, H. Wang, S. Chen, X. Quan, H. Yu, W. Choi, G. Zhang, B. Kim and J. G. Chen, *Nat. Commun.*, 2020, **11**, 2455.

110 D. Karapinar, N. T. Huan, N. Ranjbar Sahraie, J. Li, D. Wakerley, N. Touati, S. Zanna, D. Taverna, L. H. Galvão Tizei, A. Zitolo, F. Jaouen, V. Mougel and

This journal is © The Royal Society of Chemistry 2024

J. Mater. Chem. A, 2024, **12**, 19663–19684 | **19683**

M. Fontecave, *Angew. Chem., Int. Ed.*, 2019, **58**, 15098–15103.

111 H. Xu, D. Rebollar, H. He, L. Chong, Y. Liu, C. Liu, C.-J. Sun, T. Li, J. V. Muntean, R. E. Winans, D.-J. Liu and T. Xu, *Nat. Energy*, 2020, **5**, 623–632.

112 S. A. Francis, J. M. Velazquez, I. M. Ferrer, D. A. Torelli, D. Guevarra, M. T. McDowell, K. Sun, X. Zhou, F. H. Saadi, J. John, M. H. Richter, F. P. Hyler, K. M. Papadantonakis, B. S. Brunschwig and N. S. Lewis, *Chem. Mater.*, 2018, **30**, 4902–4908.

113 A. R. Paris and A. B. Bocarsly, *ACS Catal.*, 2017, **7**, 6815–6820.

114 A. R. Paris and A. B. Bocarsly, *Faraday Discuss.*, 2019, **215**, 192–204.

115 Y. Zhou, A. J. Martín, F. Dattila, S. Xi, N. López, J. Pérez-Ramírez and B. S. Yeo, *Nat. Catal.*, 2022, **5**, 545–554.

116 K. U. D. Calvinho, A. B. Laursen, K. M. K. Yap, T. A. Goetjen, S. Hwang, N. Murali, B. Mejia-Sosa, A. Lubarski, K. M. Teeluck, E. S. Hall, E. Garfunkel, M. Greenblatt and G. C. Dismukes, *Energy Environ. Sci.*, 2018, **11**, 2550–2559.

117 S. Banerjee, A. Kakekhani, R. B. Wexler and A. M. Rappe, *ACS Catal.*, 2021, **11**, 11706–11715.

118 A. T. Landers, M. Fields, D. A. Torelli, J. Xiao, T. R. Hellstern, S. A. Francis, C. Tsai, J. Kibsgaard, N. S. Lewis, K. Chan, C. Hahn and T. F. Jaramillo, *ACS Energy Lett.*, 2018, **3**, 1450–1457.

119 M. Esmaeilirad, Z. Jiang, A. M. Harzandi, A. Kondori, M. Tamadoni Saray, C. U. Segre, R. Shahbazian-Yassar, A. M. Rappe and M. Asadi, *Nat. Energy*, 2023, **8**, 891–900.

120 S. Lee, D. Kim and J. Lee, *Angew. Chem., Int. Ed.*, 2015, **127**, 14914–14918.

121 L. R. L. Ting, R. García-Muelas, A. J. Martín, F. L. P. Veenstra, S. T. Chen, Y. Peng, E. Y. X. Per, S. Pablo-García, N. López, J. Pérez-Ramírez and B. S. Yeo, *Angew. Chem., Int. Ed.*, 2020, **59**, 21072–21079.

122 Y. Zhou, R. Ganganahalli, S. Verma, H. R. Tan and B. S. Yeo, *Angew. Chem., Int. Ed.*, 2022, **61**, e202202859.

123 B. M. Tackett, E. Gomez and J. G. Chen, *Nat. Catal.*, 2019, **2**, 381–386.

124 L. Fan, Y. Zhao, L. Chen, J. Chen, J. Chen, H. Yang, Y. Xiao, T. Zhang, J. Chen and L. Wang, *Nat. Catal.*, 2023, **6**, 585–595.

125 A. N. Biswas, Z. Xie, R. Xia, S. Overa, F. Jiao and J. G. Chen, *ACS Energy Lett.*, 2022, 2904–2910.

126 J. Zhang, X. Kang, Y. Yan, X. Ding, L. He and Y. Li, *Angew. Chem., Int. Ed.*, 2024, **63**, e202315777.

127 G. Mei, Y. Lu, X. Yang, S. Chen, X. Yang, L.-M. Yang, C. Tang, Y. Sun, B. Y. Xia and B. You, *Angew. Chem., Int. Ed.*, 2024, **63**, e202314708.

128 Q. Li, D.-D. Ma, S. Zhou, W.-B. Wei, S.-G. Han and Q.-L. Zhu, *Adv. Funct. Mater.*, 2024, **34**, 2316187.

129 M. G. Lee, X.-Y. Li, A. Ozden, J. Wicks, P. Ou, Y. Li, R. Dorakhan, J. Lee, H. K. Park, J. W. Yang, B. Chen, J. Abed, R. dos Reis, G. Lee, J. E. Huang, T. Peng, Y.-H. (Cathy) Chin, D. Sinton and E. H. Sargent, *Nat. Catal.*, 2023, **6**, 310–318.

130 Z. Xie, E. Huang, S. Garg, S. Hwang, P. Liu and J. G. Chen, *Nat. Catal.*, 2024, **7**, 98–109.

131 G. Tian, X. Liu, C. Zhang, X. Fan, H. Xiong, X. Chen, Z. Li, B. Yan, L. Zhang, N. Wang, H.-J. Peng and F. Wei, *Nat. Commun.*, 2022, **13**, 5567.

132 G. Tian, Z. Li, C. Zhang, X. Liu, X. Fan, K. Shen, H. Meng, N. Wang, H. Xiong, M. Zhao, X. Liang, L. Luo, L. Zhang, B. Yan, X. Chen, H.-J. Peng and F. Wei, *Nat. Commun.*, 2024, **15**, 3037.

133 Y. Zhu, Z. Huang, Q. Chen, Q. Wu, X. Huang, P.-K. So, L. Shao, Z. Yao, Y. Jia, Z. Li, W. Yu, Y. Yang, A. Jian, S. Sang, W. Zhang and X. Zhang, *Nat. Commun.*, 2019, **10**, 4049.

134 C. de Carvalho and M. Caramujo, *Molecules*, 2018, **23**, 2583.

135 L. Chen, C. Tang, Y. Zheng, E. Skúlason and Y. Jiao, *J. Mater. Chem. A*, 2022, **10**, 5998–6006.

136 S. Berardi, S. Drouet, L. Francàs, C. Gimbert-Suriñach, M. Guttentag, C. Richmond, T. Stoll and A. Llobet, *Chem. Soc. Rev.*, 2014, **43**, 7501–7519.

137 S. A. Bonke, M. Wiechen, D. R. MacFarlane and L. Spiccia, *Energy Environ. Sci.*, 2015, **8**, 2791–2796.

138 Y. Liu, P. Cruz-Morales, A. Zargar, M. S. Belcher, B. Pang, E. Englund, Q. Dan, K. Yin and J. D. Keasling, *Cell*, 2021, **184**, 1636–1647.

139 T. Haas, R. Krause, R. Weber, M. Demler and G. Schmid, *Nat. Catal.*, 2018, **1**, 32–39.

140 P. Zhang, K. Chen, B. Xu, J. Li, C. Hu, J. S. Yuan and S. Y. Dai, *Chem*, 2022, **8**, 3363–3381.

19684 | *J. Mater. Chem. A*, 2024, **12**, 19663–19684

This journal is © The Royal Society of Chemistry 2024